Predictive Modeling of Evoked Intracranial EEG Response to Medial Temporal Lobe Stimulation in Patients with Epilepsy

Gagan Acharya[1], Kathryn A. Davis[2,3,4], and Erfan Nozari[1,5,6,*]

[1] *Department of Electrical and Computer Engineering, University of California, Riverside, CA, USA*
[2] *Department of Neurology, Hospital of the University of Pennsylvania, Philadelphia, Pennsylvania, USA*
[3] *Center for Neuroengineering and Therapeutics, University of Pennsylvania, Philadelphia, Pennsylvania, USA*
[4] *Department of Bioengineering, University of Pennsylvania, Philadelphia, Pennsylvania, USA*
[5] *Department of Mechanical Engineering, University of California, Riverside, CA, USA*
[6] *Department of Bioengineering, University of California, Riverside, CA, USA*
[*] *Corresponding author (email: erfan.nozari@ucr.edu)*

Abstract

Despite over a decade of promising results, closed-loop neurostimulation for the treatment of drug-resistant epilepsy (DRE) still relies on manual parameter tuning and yields unpredictably variable outcomes. Fully automated algorithms with predictable outcomes have remained a theoretical possibility, mainly due to a lack of generalizable models of the brain's dynamic network response to stimulation under varying parameters. In this work, we study predictive dynamical models of human intracranial EEG (iEEG) response under parametrically-rich neurostimulation and develop models that are predictively accurate and biologically interpretable. Using data from $n = 10$ subjects, we show that evoked iEEG dynamics are best explained by stimulation-triggered switched-linear models with approximately 300ms of causal historical dependence. These models are highly consistent across stimulation amplitudes and frequencies, including STIM OFF durations, which allows for learning a single generalizable model from abundant STIM OFF and limited STIM ON data. Despite significant heterogeneity among subjects, we observed a consistent distance-dependent pattern whereby stimulation impacts the actuation site and nearby regions ($\lesssim$ 20mm) directly with little or no network mediation, reaches medium-distance regions (20 $\sim$ 100mm) indirectly through network interactions and hardly reaches more distal areas ($\gtrsim$ 100mm). Peak involvement of network interactions occurs at about 60-80mm from the stimulation site. Due to their predictive accuracy and mechanistic interpretability, these models have far-reaching applications in model-based seizure forecasting and stimulation design for closed-loop neurostimulation.

1 Introduction

Closed-loop neurostimulation has long been considered a promising alternative to highly invasive resection surgery for individuals with drug-resistant epilepsy. Extensive research over the past decades has highlighted its numerous advantages, including short-term benefits like electric stimulation-induced desynchronization of neuron firing to counteract seizures, as well as long-term benefits such as the modification of cortical excitability via neuroplasticity [1, 2]. Nevertheless, its state-of-the-art clinical implementation, the RNS®system from NeuroPace, Inc. [1] has known limitations, including a lack of mechanistic understanding [3], simplistic detection algorithms, and non-adaptive pre-selected stimulation parameters [1, 4, 5]. As a result, though highly effective in some individuals, RNS outcomes vary widely among patients, and only 18% of those receiving RNS implantation experience seizure freedom for a period of 1 year or longer [6]. To establish neurostimulation as a robust treatment with predictable outcomes, it is vital to have *the ability to predict* the future trajectory of neural activity, both in the absence and presence of neurostimulation. Such predictive modeling, in particular, opens the door to a host of model-based detection and control algorithms that have been developed and studied for decades in engineering [7–9] but often need accurate predictive models to succeed.

Despite decades of research, accurate predictive models of an epileptic brain's response to neurostimulation are largely lacking. A large group of studies have developed models that primarily provide explanations for the disorder on a phenomenological level [10–13]. These models have been used

for extracting features in seizure detection algorithms [14–21], conducting stability analysis [8, 22], and localizing seizures [23]. However, these models are not tuned using subject-specific stimulation data and are thus inadequate for robust and predictable closed-loop control design over the diverse set of parameters for neurostimulation [8, 9]. A second body of work has pursued more accurate and/or subject-specific models using detailed finite-element modeling of the brain's electromagnetic response to neurostimulation [24–27]. This is often done in conjunction with biophysical modeling and used for the analysis and optimization of the impact of electrode placement and (de)polarization activity of neuronal tissue. Nevertheless, these models are often not built for and capable of accurate time-series prediction, particularly at a large-scale network level beyond the local stimulation site.

Finally, a third body of work has specifically pursued data-driven predictive modeling of the brain's response to neurostimulation. Multiple studies have used linear autoregressive models to fit the neural activity triggered by neurostimulation [28–31] while others have opted for nonlinear kernel-based autoregressive modeling [32, 33]. However, these works have mainly focused on univariate modeling (i.e., modeling the neurostimulation-evoked response at a single measurement source), while modeling the evoked *network response* has remained more challenging [34–36]. Furthermore, a significant portion of these studies relies on simulated data, data from non-human primates, or data in the absence of stimulation. As such, accurate subject-specific predictive models of brain network dynamics under neurostimulation have remained largely lacking.

In this study, we present a rigorous data-driven framework for developing subject-specific network dynamical models of intracranial electroencephalography (iEEG) dynamics in the absence and presence of medial temporal lobe deep brain stimulation in patients with epilepsy. We use recordings from the Restoring Active Memory (RAM) Public dataset, which offers a particularly rich resource for data-driven modeling due to the presence of factorial parameter search experiments where multiple stimulation parameters are varied in extensive combinations. We follow a standard system identification approach [37] where models are compared based on the accuracy of their one-step-ahead predictions (namely, predictions of iEEG measurements at any sample t based on all the available histories of past iEEG and stimulation data up to sample $t-1$). This emphasis on predictive modeling is not only essential for closed-loop seizure prediction and suppression, as noted earlier, but also provides the means for *studying Granger causality* among the input (neurostimulation) and output (iEEG) variables, as described next.

2 Results

Model. The ability of any computational model in explaining data depends heavily on its chosen structure. In this work, unless when otherwise stated, we use a bilinear model of the form

$$\Delta y_k(t) = (A_k + \mathcal{U}(t)C_k)Y_k^L(t) + B_k U_k^M(t) + \sum_{\substack{i=1 \\ i\neq k}}^{C} D_k^i Y_i^P(t) \quad (1)$$

to model individualized (subject and channel-specific) iEEG response to DBS. In this model, the one-step change in the iEEG activity of the kth channel, i.e., $\Delta y_k(t) = y_k(t+1) - y_k(t)$, is predicted linearly based on the past L samples $Y_k^L(t)$ of iEEG in that same channel, the past M samples $U_k^M(t)$ of stimulation input, the past P samples $Y_i^P(t)$ of iEEG in other channels, and the bilinear interactions $\mathcal{U}Y_k^L(t)$ between the stimulation input and iEEG output (cf. Methods for details). This bilinear choice of the model structure is motivated by the long history of bilinear modeling in neuroscience [38] as well as our prior work showing the linearity of resting state (i.e., STIM OFF) iEEG [39]. We thus depart from linearity towards highly complex models (e.g., deep neural networks) gradually and only to the extent supported by data. Bilinear models provide a natural first step in moving beyond linearity [40–42] and are thus preferred unless more complex models provide substantial improvement in accuracy, a topic to which we will return later (cf. Figure 6b).

iEEG data contains about 300ms of causal historical dependence, despite significant heterogeneity across subjects and channels. Unlike models with latent states such as linear state-space models [37, 43] or hidden Markov models [44], autoregressive models predict future outputs based on the history (lags) of *observed* data, i.e., inputs and outputs. This creates a trade-off, where AR models have significantly larger state dimensions in return for having the state fully observed (and therefore known more accurately) and interpretable. A critical structural parameter for AR models is thus the amount of input and output history used for prediction. Notably, this is different from and can be

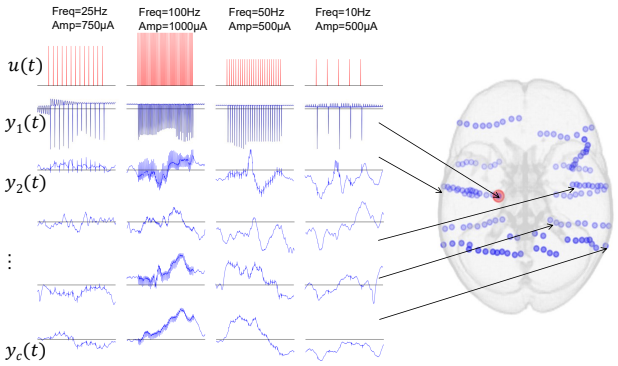

Figure 1: Illustration of the iEEG data used in this work for a sample subject (see Methods for details). Each cluster of adjacent blue circles correspond to contacts on a single electrode (warped due to registration to standard space). $u(t)$ encodes the applied stimulation pulse train, including both its frequency and amplitude. $y_k(t)$ refers to the recorded iEEG signal of the kth electrode ordered based on its closeness to the stimulation site.

significantly smaller than, the decay of iEEG autocorrelation. While the latter answers the question of whether the output at two separate time points is merely *correlated*, the former answers a *causal* question, in the Granger sense of causality [45], of whether any piece of data in the past provides *additional information* beyond what is available in the less-distant past.

Figure 2a shows how autoregressive models with different amounts of autoregressive (L) and input (M) history compare across all subjects and channels. In general, the amount of historical dependence that gives the highest predictive accuracy greatly varies among subjects and even different channels within each subject. In fact, for almost all combinations of L and M, we can find at least one subject-channel where that combination is optimal. This vast heterogeneity exists regardless of the statistical measures for comparison (mean- or median-based), and reinforces the need for *sub-individualized* data-driven modeling, as opposed to normative models which explain seizure dynamics generically. In what follows, we evaluate each model on the basis of its 'win rate', i.e., the percentage of subject-channels for which that model had the smallest cross-validated predictive accuracy.

Increasing the amount of autoregressive history (L) almost monotonically improves predictive accuracy, but only marginally so beyond 200-300ms. Specifically, models with larger L have larger win rates across subjects and channels (Figure 2b, bar plot), but increasing autoregressive history from 300 to 500ms only improves win rate by 10% (Figure 2b, dashed horizontal line). This trend can also be seen from average prediction error (average normalized MSE across all subjects and channels), which drops significantly when increasing L from 1ms to 50ms and decays fairly notably until about 200-300ms but saturates thereafter (Figure 2b, solid line).

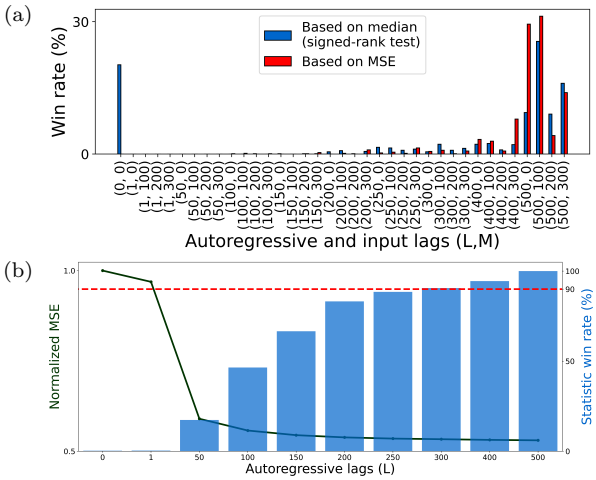

Figure 2: **Model order distribution and performance across subjects and channels.** For each subject-channel, we trained ARX models of various orders (L, M) ($L \in \{0, 1, 50, 100, ..., 500\}$ and $M \in \{0, 100, 200, 300\}$) and determined the pair (L, M) that resulted in the model with the *best* fit over unseen data. (a) We plotted the *Win rate* i.e., the percentage of times each (L, M) pair is the *best* across all considered channels ($n = 1171$). We used 2 definitions of the *best* model: based on the mean ((L, M) pair that resulted in the lowest MSE) and based on the median ((L, M) pair that is superior to other model orders as per Wilcoxon signed-rank test (see Methods)). Irrespective of the definition used, we saw that larger autoregressive lags (i.e., $L \geq 400$) are favored across more than 90% channels. About 66% of the modeled channels favored a non-zero input lag (i.e., $M > 0$) and hence are causally affected by direct stimulation input. (b) We also plotted the validation MSE (averaged across all M) as a function of the autoregressive lags (L) (left y-axis) and found that although a larger L is more favored, doing so only resulted in a marginally better fit in comparison to a model with 200 to 300 autoregressive lags. In the same figure, we also plot (right y-axis) the 'statistical win rate', defined as the percentage of channels where a model of order L has an MSE that is statistically similar (i.e., within $\pm 2S.E.M$) to the MSE corresponding to the best model. From this plot, we observed that a model with $L = 300$ is sufficient for 90% of all the channels.

Unlike autoregressive history, the amount of past input history (M) that has a causal effect on evoked iEEG response varies greatly among subjects and channels (Figure 2a). For about two-thirds of the subject-channels, some (though still heterogeneous) amount of input history improves predictive accuracy, while for other subject-channels inclusion of any amount of input history, even from the immediate past, lowers predictive accuracy. This lack of direct causal effect in the latter group is consistent with the hypothesis that not all channels are directly excited by stimulation, but rather receive the impact of stim-

ulation through complex spatiotemporal interactions with other channels. Such network-mediated stimulation effects may also be small enough to be statistically undetectable compared to baseline fluctuations [39], characterizing a group of subject-channels with no evoked response, whether direct or indirect (see also Figure 5).

Given the relatively fast sampling rate of iEEG (1000Hz), it is also possible that successive input/output samples contain redundant, correlated information and need not all be included in the model. To test this hypothesis, we compared the above-described models with densely-sampled input-output history against sparsely-sampled alternatives where both the input and output are sampled every τ milliseconds ($\tau > 1$). The same number of lags was used across the dense and sparsely sampled models to ensure fair comparisons. As seen in Figure 3, dense models achieve higher predictive accuracy, even though sparse models with the same number of lags have access to a wider window for prediction (τLms for a sparse model compared to Lms in a dense model). In particular, this result *discourages the use of delay embedding* [46] despite its theoretical appeal [47], and instead encourages investing the available computational power (which is often extremely limited in chronic implants) into learning temporally short-range predictive relationships.

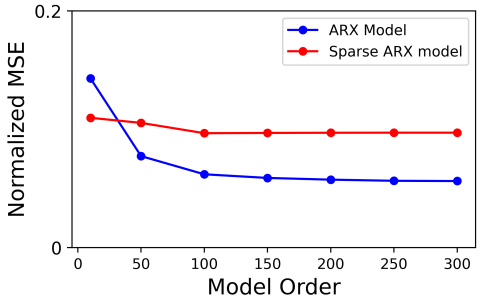

Figure 3: **Effect of sparser temporal sampling of autoregressive lags on model accuracy.** For each channel in the data, we considered 2 categories of models: ARX models with *dense temporal sampling* (i.e., iEEG lags are spaced 1ms apart) and ARX models with *sparse temporal sampling* (i.e., iEEG lags are spaced $\tau > 1$ms apart). For the latter, the exact sampling time τ was chosen separately for each channel based on delay embedding theory using the method described in [48]. We trained sparse and dense models of various lags ($L \in 1, 50, 100, 150, 200, 250, 300$) and plotted the normalized MSE across subject-channels as a function of L. Although the sparse ARX model with L lags has access to a much larger duration of iEEG history (i.e., τLms) in comparison to a dense model (i.e., Lms), the former has lower accuracy. Thus, temporally short-range models with higher sampling rates are more predictive.

iEEG evoked response is best described by switched-linear dynamics. The functional form, extent, and even the very presence of nonlinearity in the neural dynamics of patients with epilepsy has been the topic of much debate [49, 50]. In our recent work [39], we showed that resting state (interictal, STIM OFF) iEEG dynamics are best described by linear autoregressive models. However, our examination of STIM ON and STIM OFF periods reveals notable distinctions in the optimal autoregressive parameters (i.e., matrix A_k in Eq. (1)) when fit separately for each duration. Therefore, we first sought direct evidence for whether the presence of stimulation makes iEEG dynamics nonlinear. We tested if matrix A_k trained using resting state data (i.e., STIM OFF) can generalize over STIM ON durations. We did this by comparing 2 linear models across each subject: (1) an ARX model trained over STIM ON duration (Stim Model in Figure 4a) and (2) the Stim Model with the A_k matrix replaced with that trained using STIM OFF data (RS Model in Figure 4a). If the dynamics in the STIM ON and STIM OFF durations were indeed similar, we could expect the above 2 models to perform similarly when we test them on unseen data. Moreover, an agreement between these models would indicate that the iEEG dynamics can be captured largely by a single linear model. However, our analysis in Figure 4a and 4b showed that the Stim Model performs significantly better on unseen data than the RS Model and thus indicated the presence of stimulation-induced nonlinearity.

Arguably, the simplest nonlinear choice to account for the observed differences between STIM ON and STIM OFF dynamics is a switched-linear model that simply switches between one linear model during STIM ON and another linear model during STIM OFF. This is also a special case of the bilinear model in Eq. (1), wherein the gating term $\mathcal{U}(t) = 1$ if t is within a stimulation duration and 0 otherwise. A direct comparison between ARX and switched ARX models showed that the switched ARX model was favored over its linear counterpart for the majority of subject-channels, as illustrated in Figure 4c.

Nevertheless, the comparison of the descriptive ability of a switched-linear model to that of a simple linear model has to be made from a more nuanced level taking into account the potentially confounding effects of other model attributes, such as the presence of network interactions and direct STIM effect. Motivated by this, we compared a host of linear models, such as the VARX model (linear ARX model with network interactions) or AR model (linear AR model), with their switched-linear counterparts. As shown in Figure 5a, independent of the

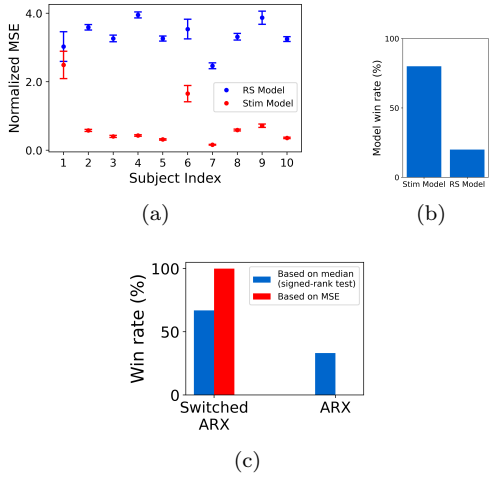

Figure 4: **Evidence of nonlinear dynamics and switching behavior.** We tested an ARX model trained using STIM ON (Stim model) data against a similar model with the A_k matrix replaced by that trained using STIM OFF data (Resting State (RS) model). (a) The performance (MSE) difference between these models and (b) their respective win rates, indicating the presence of stimulation-dependent nonlinearity. (c) When we account for the nonlinearity using a switched ARX model, we found it to be more descriptive of the iEEG response in comparison to a single ARX model

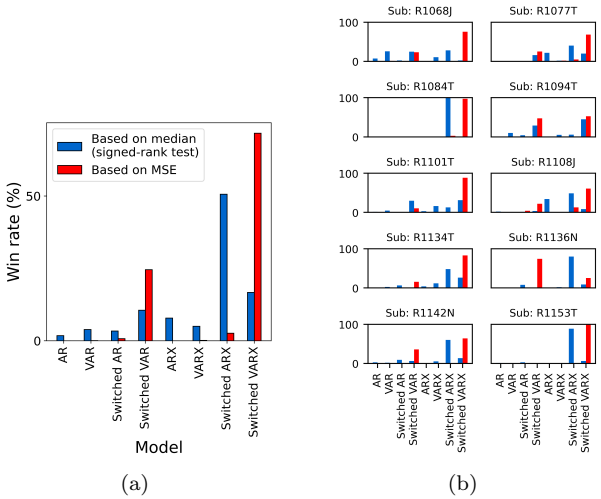

Figure 5: **Comparison of linear and switched-linear models.** (a) Win-rate distribution across all subjects and channels. Irrespective of the criterion used, switched-linear models were observed to outperform linear models for more than 90% of the channels. The preference for modeling the causal effects of stimulation and network interactions seemed to vary greatly among channels. (b) A zoomed-in version of the plot in (a) shows the subject-wise distributions of the model win rate.

statistical measure for comparison (mean or median), the switched-linear class of models is more consistent with the data in the vast majority of cases. That being said, there is still vast heterogeneity among subjects and channels in what kind of switched-linear model achieves the highest predictive power, while even some (about 10%) of subject-channels are best described by a single linear model throughout all STIM ON and STIM OFF durations. The distributions of win rates for each subject also show a consistent preference for switched-linear models across all subjects, even though vast heterogeneity also persists in these distributions, both within and between subjects (Figure 5b).

A further aspect of the large heterogeneity in the channel models in Figure 5 is whether stimulation has a direct causal effect on iEEG evoked response. We observed that stimulation effects are predominant in more than 75% cases across subject-channels. This observation was further validated when we conducted a bootstrapping experiment (see Methods) over the input lags and found empirical evidence for direct stimulation effects in about 95% of the 75% subject-channels considered in the test.

Despite the higher predictive accuracy of switched-linear models compared to linear ones, their binary gating enforces a single linear model for all STIM ON durations, irrespective of the stimulation's frequency and amplitude. A fully bilinear model with $\mathcal{U}(t) = [U_k^M(t)]^\intercal$ in the form described by equation Eq. (1) can potentially alleviate this issue by allowing the stimulation waveform to directly modulate the linear dynamics using the interaction term $\mathcal{U}(t)C_kY_k^L(t)$. A third, middle-ground alternative is to employ an amplitude-weighted switched-linear (AWSL) model where the gating term $\mathcal{U}(t)$ is determined by the amplitude of the stimulation rather than a binary signal. However, we found the switched-linear model to be more consistent with the data compared to the more complex bilinear and AWSL alternatives (Figure 6). This is remarkable not only from a biological perspective, but also from an engineering perspective given the large body of literature on control design for switched linear systems [51].

While we notice the lack of benefit in bilinear over switched-linear models, this does not remove the possibility that significantly more complex models still explain stimulation-evoked iEEG response better. When compared against some of the most commonly known nonlinear models, switched-linear models were highly predictive across channels, second only to feedforward Artificial Neural Networks (ANNs) with *ReLU* activation. Note, also, that ANNs with *ReLU* activation are also switched-linear models. In fact, when compared against ANNs with *tanh* nonlinearity, those with *ReLU* activations explained the data significantly better. Nevertheless, compared to a sim-

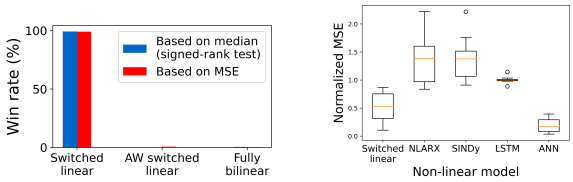

(a) (b)

Figure 6: **Comparison of switched-linear models with other forms of nonlinear models.** (a) We compared the switched-linear model against an amplitude-weighted (AW) switched-linear model and a fully-bilinear model. As indicated by the win rate across, we found switched-linear models to be most predictive across all subject-channels (b) When we compared switched-linear to other forms of nonlinear models, we found that the artificial neural networks (ANNs) resulted in the lowest MSE and this result was followed by the switched-linear model.

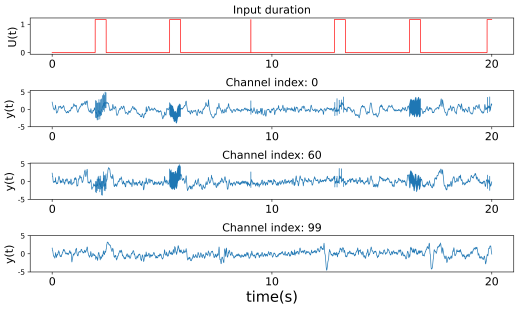

Figure 7: **Heightened activity in channels without direct causal effect from the stimulation.** (a) Plot showing the STIM ON durations within a specific stretch of the recordings. In (b)-(d), we plot the iEEG activity in response to the stimulation signal in (a) for 3 channels that did not show any evidence of being directly affected by the applied stimulation.

ple switched-linear model in Eq. (1), the ANNs with *ReLU* activation have two orders of magnitude more parameters, combinatorially more switching regions, and almost no biological interpretability. This makes the former, simpler switched-linear model potentially preferred for mechanistic understanding and model-based closed-loop seizure stabilization, particularly in chronic implants with limited logic gates and battery resources.

Network-mediated DBS spread is consistently distance-dependent. A critical feature in the dynamics of any iEEG channel is network interactions with other channels, both from a network control perspective as well as a mechanistic understanding of how stimulation effects spread throughout the brain. Network interactions are captured by the term $\sum_{\substack{i=1 \\ i \neq k}}^{C} D_k^i Y_i^P(t)$ in Eq. (1), where we refer to models with at least one nonzero D_k^i (at least one nonzero effective connectivity between two electrodes) as *vector* autoregressive (VAR). In our recent work [39], we found VAR models to be *less*, not more, predictive of resting state iEEG compared to models with no network interactions (all $D_k^i = 0$), indicating a lack of causal effects among the channels at rest.

The presence of stimulation, on the other hand, has the potential to boost causal network interactions through which the stimulation effect can spread. As noted earlier (cf. Figure 2a), across all subjects, we found no *direct* causal effect from stimulation input to about 25% of the channels. Nevertheless, several of such channels still demonstrate clearly heightened activity during STIM ON periods, therefore hinting at an *indirect* causal effect of stimulation mediated by network interactions (Figure 7).

Assuming that the spread of the stimulation through the brain connectome is the main reason for the significance of network effects in STIM ON durations compared to resting state periods, then the stimulation channel itself should have no causal network effect *from* other channels. Therefore, we hypothesize that response at the site of stimulation can be best explained by a switched-linear model without network interactions (i.e., switched ARX). This was indeed the case when we compared switched VARX and switched ARX models trained for stimulation channels, and found that the latter model was favored in 8 out of the 10 subjects in our data. Even for the 2 subjects where switched VARX was favored, we found that the relative improvement in MSE from incorporating data from other channels was only modest ($< 10\%$). Interestingly, this is consistent with the role played by the do-operator in causal discovery [52], effectively isolating the anode from being causally influenced by other nodes within the network.

Analyzing the channels corresponding to electrodes that were directly stimulated, we consistently found that these non-stimulated channels most often receive causal effects from other nodes in the network. More interestingly, however, we found that the strength of this causal effect (i.e., the amount of added model predictive power when including the past history from other channels) varies in a consistently distant-dependent manner. At one extreme, we observed that the strength was least pronounced for electrodes located in close proximity to the anode. This indicates that the response in these channels, similar to the stimulated channel itself, is mostly overpowered by direct stimulation effects. On the other extreme are nodes that receive little to no effect from stimulation, whose network interactions are expectedly similar to

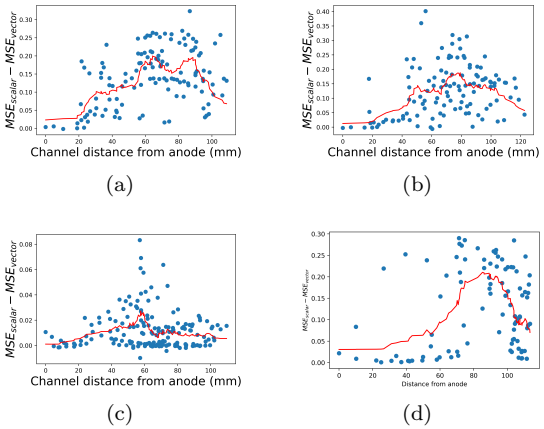

Figure 8: **Strength of network interactions as a function of distance from the stimulation site.** The strength of causal effects from other nodes (channels) in the network to each node is measured by the MSE advantage $MSE_{scalar} - MSE_{vector}$, where the former (latter) comes from a model in which the history of other nodes' iEEG values is not (is) used for one-step-ahead prediction. (a)-(d) The MSE advantage for each channel as a function of its distance to the stimulation site (shown in blue) across 4 different subjects. We found that the distance-based moving average of this advantage (shown in red) is initially close to 0, rises with distance until about 70mm, and then decreases thereafter.

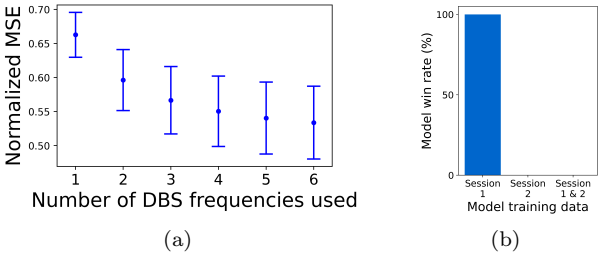

Figure 9: **Generalizability of trained models across stimulation frequencies and sessions.** (a) We plotted the normalized test MSE as a function of the number of stimulation frequencies used as part of the training set. We found that including more frequencies results in a more generalizable model. (b) However, we did not find it to be beneficial when we extend the dataset using recordings from multiple sessions. Specifically, when we considered 2 sessions and the 3 possible models that can be trained from them (using only session 1 or only session 2 or both in the training set), we found that unseen data from session 1 was best predicted by the model trained on data from Session 1 only.

weak/insignificant network interactions during resting state found earlier [39]. At an intermediary Euclidean distance from the anode (around 70mm) were nodes that received the strongest causal effect from network interactions.

Evoked iEEG dynamics are highly consistent across stimulation frequencies but less consistent across sessions. A critical challenge for model-based control design for neurostimulation is learning models that generalize beyond the (past) data over which they are trained, particularly given the extreme inter and intra-subject variability in epilepsy on the one hand and scarcity of stimulation data on the other. One aspect of such generalizability is across responses to different stimulation frequencies, which is not trivial given that various stimulation frequencies elicit unique inhibitory and excitatory responses [36]. We performed a large-scale combinatorial experiment wherein we trained models for each channel using a dataset with k of the 6 stimulation frequencies (including 0Hz, i.e., STIM OFF durations) and validated the models on a test dataset containing all the 6 frequencies. Figure 9 shows the normalized MSE for different values of k, averaged across all channels and $\binom{6}{k}$ possible models for each value of k. We found that using a training dataset with a higher variety of stimulation frequencies proves advantageous in learning a more generalizable model. In particular, the inclusion of 0Hz stimulation (STIM OFF data) in training data resulted in a better model. Given the abundance of such STIM OFF recordings across various datasets, our result indicates that such data can be leveraged to learn more accurate models of stimulation-evoked response models. Additionally, the saturation of the MSE with just 6 frequencies indicates that it is possible to learn a predictive model with a relatively safe and simple experimental design.

Another important aspect of the generalizability is that across temporally-spaced sessions. If brain dynamics were to be stationarity across different sessions, combining the data directly from these sessions should result in a superior model compared to fitting a model using data from only one session. We thus compared 3 types of switched-linear models over 2 different recording sessions: a model trained on Session 1, a model trained on Session 2, and a third model trained on both sessions. When these models were tested using unseen data from one of the sessions (Session 1), we found the model trained on data only from that session to be the most predictive. This was in fact the case in all 10 subjects. This finding thus indicates the presence of non-stationary or time-varying behavior across sessions. Therefore, models trained over a prior session cannot be directly deployed in a new session, but have to be re-trained continuously to make sure they remain predictive.

3 Discussions

In this study, we presented a data-centered framework for modeling the iEEG response induced by intracranial neurostimulation. We highlighted the effectiveness of switched-linear autoregressive models with about 300ms length of history in accurately representing seizure-free iEEG dynamics throughout the pre-STIM to post-STIM duration. Furthermore, we elaborated on efficient methodologies for training such models without requiring supplementary information. We analyzed the models and channels from the standpoint of causal effects of stimulation, both direct and indirect. In addition to the modeling, we experimentally characterized the generalizability of the system identification process across different stimulation frequencies and recording sessions.

Our focus on iEEG in this work stems from its importance and gold-standard role as a feedback signal for closed-loop intracranial neurostimulation. In the context of epilepsy, iEEG has long been used for the localization of the seizure onset zone (SOZ) [53], and subnetworks extracted purely from iEEG data using unsupervised machine learning have been shown to be able to differentiate between SOZ and non-SOZ regions [7, 54] as well as pre-ictal, onset, and ictal durations [8]. Furthermore, the general predictive modeling methodology used in this study is not restricted to iEEG and can be used, subject to proper modifications, with other forms of neurophysiology and neuroimaging data (see, e.g., [39]).

A rather undesirable aspect of iEEG recordings in general is the presence of stimulation artifacts [36] and epileptic discharges. From the perspective of understanding brain function, it is common practice to remove any such effect, often conservatively, and only consider the "clean" data for modeling and analysis [55, 56]. However, when modeling the brain for the purpose of closed-loop detection and control, we need models that accurately capture all the effects and elements that appear in the control loop, including all durations (pre-STIM, STIM ON, post-STIM) and regions (SOZ and non-SOZ, gray and white matter). We can no longer afford to disregard numerous channels and recording durations, as often happens during common iEEG preprocessing. Therefore, we adopt a minimal pre-processing pipeline (cf. Methods) and delegate the task of handling complexities in the data to the data-driven model.

An important aspect of our findings is the vast heterogeneity among optimal model structures (let alone parameters) among subjects and even channels within the same subject. This is understandable considering the variations in input effects and the diverse network influences across channels, and only reinforces the need for individualized analysis and treatment in epilepsy [57]. We even observe sufficient heterogeneity among the dynamics of different recording sessions from the same individual to prevent a model tuned to one session from properly generalizing to another. This is conceptually similar to the well-known lack of stability of intracranial multi-unit activity recordings across sessions [58] but is observed at a significantly larger spatial scale where the physical drift of the recording electrodes relative to the surrounding tissue is less to blame. Nevertheless, across scales, such non-stationarity necessitates adaptive detectors and controllers with constant re-tuning of models and algorithms [59, 60].

Our modeling framework is similar to Dynamic Causal Modeling (DCM) [61] in a number of respects. Bilinear families of dynamic models have a long history in DCM, and switched-linear models with a STIM ON/OFF switching signal are conceptually similar to works that build separate DCM models for STIM ON and STIM OFF periods [41, 62]. Nevertheless, we depart from DCM in a number of ways, including a prediction-error-based parameter estimation methodology [37] instead of the variational Bayes methodology used in DCM [63]. Furthermore, DCM typically uses *single-lag* bilinear models for fMRI [41] and complex neural mass models for EEG [64], whereas we show the power of bilinear autoregressive models *with long input-output histories* in explaining EEG dynamics. These modifications not only make the resulting models more predictively accurate but also significantly more scalable to large-scale recordings. Similar hybrid modeling approaches have also been done for autoregressive models in works such as [40] and provide a broad rationale for the models described in this paper.

In the context of system identification [37], the experiment design process holds significant importance for and essentially limits the achievable accuracy of any downstream modeling. A good experiment design process involves probing the system with a *persistently exciting* or a diverse set of input frequencies in order to record all the possible dynamical modes of the system [37]. This may even be more important for the brain, as it has been suggested that different stimulation frequencies can result in distinct types of responses, with lower frequencies (10-60 Hz) typically inducing inhibitory effects and higher frequencies (100-200 Hz) producing excitatory responses [36]. Thus, it becomes crucial to incorporate a diverse range of stimulation parameters before modeling. Nevertheless, the conventional approach to experimental design in human studies [38, 40] often

entails repeatedly applying a single, fixed-parameter stimulation. This will allow the models to simply "memorize" the brain's response to that specific stimulation, without necessarily learning anything generalizable about the brain's response to neurostimulation. The RAM Parameter Search recordings used in this study is one of very few that encompasses a wide range of stimulation frequencies, amplitudes, and durations. Nevertheless, this dataset is not ideal either, e.g., due to a lack of recordings where changes in stimulation parameters occur without going through a STIM OFF phase. While recent works such as that in [34] have attempted to construct more parameter-rich experiments for non-human primates, similar efforts toward modeling the human brain are largely absent. Nevertheless, the ability to learn predictive models using the RAM dataset, as described in our work, suggests that it is feasible to achieve successful modeling using a relatively small yet carefully chosen set of stimulation parameters.

Future steps towards the development of a complete model-based closed-loop seizure control system require even richer and more extensive datasets that encompass simultaneous seizure and neurostimulation, enabling models to learn the interactions between ictal and stimulation-evoked dynamics. Such data, however, is challenging to collect for a number of reasons. Despite ongoing advancements in seizure detection, accurately and reliably timing stimulation relative to seizure onset remains a major challenge, which is further exacerbated by the heterogeneity of seizure events even within the same individual. Further, iEEG recordings have significantly better spatial and temporal coverage and algorithmic flexibility during acute seizure monitoring, but manipulating intrinsic seizure dynamics can interfere with medical diagnostics at this stage. Animal and computational models can therefore play an invaluable role before algorithmic designs can be translated to humans.

4 Methods

Data. Throughout this work we use data from the Parameter Search experiments of the Restoring Active Memory (RAM) project, consisting of multichannel resting state, task-induced, and neurostimulation-induced iEEG responses of over 80 human subjects [65]. As reported extensively in the RAM documentation, the highest stimulation amplitude (A_{safe}) that could be applied to each subject without resulting in after discharges were first measured. This value was then used in the PS2 experiments which we use in this work, providing subjects with 500ms fixed-duration stimulations of biphasic pulse trains delivered at varying combinations of current amplitudes (3 levels: A_{safe}, $A_{safe}-0.25$mA and $A_{safe}-0.5$mA) and frequencies (single pulse, 10Hz, 25Hz, 50Hz, 100Hz, or 200Hz). Each subject has undergone multiple stimulation sessions, ranging from 2 to 5, with each session involving a different stimulus (anode-cathode) location within the medial temporal lobe (MTL). During each session, pulse trains of each combination of amplitudes and frequencies were repeatedly delivered multiple times (about 20-30 times, equivalent to 30 minutes of total experimentation). Such exhaustive repeated parameter sweep data is rare in stimulation-evoked iEEG and makes this dataset particularly rich for the modeling purposes of this study. To partly control for the great variability among subjects and the high computational cost of numerical experiments, we limited our analyses to a subset of 10 randomly chosen subjects among those with an iEEG sampling frequency of 1000Hz.

Preprocessing and data decomposition. As noted earlier (see Discussions), we used minimal preprocessing in order to build models that can capture stimulation-evoked iEEG dynamics in its full complexity. We removed power line harmonics by applying 4th-order Butterworth notch filters at 60Hz, 120Hz, and 180Hz. We then detrended the signal using a first-order polynomial fit to remove linear drifts and z-scored the data to standardize signals across all subjects and channels. Finally, we selected windows of length 1500ms around each stimulation. These consisted of 500ms pre-stim, 500ms stim, and 500ms post-stim for pulse train stimulations and 750ms pre-stim and 750ms post-stim for single-pulse stimulations. This was due to the fact that only about 1/6 of the recordings corresponded to durations where stimulation was applied. Hence, using the full recordings could (and did, based on our pilot analyses) bias the models towards fitting STIM OFF durations and ignoring evoked responses.

We define the input time-series $u(.)$ based on the stimulation timing and parameters. If a pulse train with frequency f and amplitude a was applied starting from time t_k (always lasting for 500ms), then we set $u(t_k + \Delta t) = a$ for all $\Delta t \in [0, 500]$ that are integer multiples of $1000/f$ and $u(t) = 0$ otherwise. The modulating term $\mathcal{U}(.)$ in Eq. (1) was set as $\mathcal{U}(t) = a$ (amplitude-weighted switched linear) or $\mathcal{U}(t) = 1$ (switched linear) for all t within stimulation durations $[t_k, t_k + 500]$ and $\mathcal{U}(t) = 0$ for other duration. In the case of the complete bilinear model, we set $\mathcal{U} = u$, which can be thought of as a more natural choice for modulation.

Unless otherwise stated, we split the processed iEEG recordings into training and test as follows. Each 1500ms window (corresponding to each instance of stimulation, see above) was split into 5 continuous folds of data (300ms each), out of which 4 randomly selected folds were used for training, and the remaining fold was used for testing.

Models. The main focus of our work is the dynamic model described in Eq. (1), which is used to make one-step ahead predictions about the iEEG response given past iEEG and input history lags as regression features. We denote the iEEG history of length L for channel k at time t as the vector $Y_k^L(t) = [y_k(t-1), y_k(t-2), ..., y_k(t-L)]^\intercal$. Similarly, the input lags vector $U_k^M(t)$ of length M is given by $[u(t-1), u(t-2), ..., u(t-M)]^\intercal$.

Several families of models used in this work are special cases of the model in Eq. (1). A linear autoregressive model is obtained by setting the matrices B_k, C_K, and D_k to 0. The learnable (not necessarily zero) parameter sets of the subclasses of Eq. (1) used in this work are listed in Table 1.

Model	Parameters θ
AR	$\{A_k\}$
ARX	$\{A_k, B_k\}$
VAR	$\{A_k, D_k\}$
VARX	$\{A_k, B_k, D_k\}$
BL/SL AR	$\{A_k, C_k\}$
BL/SL ARX	$\{A_k, B_k, C_k\}$
BL/SL VAR	$\{A_k, C_k, D_k\}$
BL/SL VARX	$\{A_k, B_k, C_k, D_k\}$

Table 1: Parameter sets of linear and bilinear/switched linear (BL/SL) models used in our work. Note that bilinear and switched linear models have the same set of nonzero weights and only differ in their encoding of $\mathcal{U}$ (see 'Preprocessing and data decomposition' above). In each case, the shown matrices are learned from data while matrices outside of this set are assigned to 0.

Determining the structure of Eq. (1) involves choosing appropriate model orders (L, M, and P) as well as determining the subset of $\{A_k, B_k, C_k, D_k\}$ that can be nonzero. We make all such choices in a data-driven manner. This is particularly important when we want to fit personalized models, where we need to account for the knowingly-large subject-to-subject variability [57, 66]. Given the compound and combinatorial nature of structural choices, we also use a hierarchical bottom-up approach where we tune low-level quantities (e.g., number of autoregressive lags) before selecting higher-level choices (e.g., type of nonlinearity or presence of network interactions). For each channel, we first assume an ARX model and find the pair of iEEG and input lags (i.e., L and M) that maximizes the model accuracy. Fixing the obtained values of (L, M), we train the models described in Table 1 while keeping the value of the maximum network lags P as 1. Once we statistically determine the best model structure (i.e., linear or bilinear/switched), we use it to determine the optimal value of P by evaluating the validation MSE of models fit with different values of P (increased from 1 to 100 in steps of 10).

In addition to the above models, we trained other nonlinear models, as follows:

Artificial Neural Network (ANN): A 2-layer feed-forward network with *ReLU* activation, with 500 and 50 nodes in the first and second layer respectively, and inputs being Y_k^L and U_k^M. We opted for the *ReLU* activation function due to our observation that it yielded superior performance compared to alternative nonlinear functions, such as *tanh*.

Long Short-Term Network (LSTM): Standard single layer LSTM with $y_k(t-1)$ and $u(t-1)$ as input and expected output $\Delta y_k(t)$

Sparse Identification of Nonlinear Dynamics (SINDy) using 3rd degree polynomial expansion

Nonlinear ARX (NLARX) specified in [67], model order (50, 50, 1) used for all channels

Learning. We train the free parameters of each model by minimizing the regression mean squared error

$$\text{Cost}(\theta) = \text{MSE}(\theta) + \lambda||\theta||_2^2 \tag{2a}$$

$$\text{MSE}(\theta) = \frac{1}{N}\sum_{t=1}^{N}(\Delta y_k(t) - f(X_k(t);\theta))^2 \tag{2b}$$

where $f(\cdot)$ is any of the aforementioned parametric families of models and $X_k(t)$ denotes the regression features of the tth sample and the kth iEEG channel. This may include the lags of iEEG recording of the kth channel ($Y_k^L(t)$), that of other channels ($Y_i^P(t)$), and input lags ($U_k^M(t)$). This minimization is l_2-regularized to avoid overfitting. Specifically, we added a cost of $\lambda||\theta||_2^2$ to the MSE cost function, where λ is the penalty factor and was empirically fixed to a value of 0.1.

Performance metric. We evaluated trained models over test data based on a number of metrics. One metric is test MSE which is also computed from Eq. (2) but computed over test data. Since MSE (as with any mean-based measure) can be susceptible to outliers, we also compared the models based on a one-sided Wilcoxon signed-rank test with Bonferroni correction for comparisons between multiple

pairs. Once we determine the best models for each channel across all the subjects, we define the model *win rate* for any model f_i as

$$\text{Win rate}(f_i) = \frac{\#\text{ channels where } f_i \text{ is best}}{\#\text{ total channels}}. \quad (3)$$

Sparse ARX modeling via delay embedding. When comparing dense vs. sparse autoregressive models, we compared a regular ARX model (cf. Table 1) with a sparse version

$$\Delta y_k(t) = A_k \begin{bmatrix} y_k(t-\tau_k) \\ y_k(t-2\tau_k) \\ \vdots \\ y_k(t-L\tau_k) \end{bmatrix} + B_k U_k^M(t).$$

The tuning of the delay time τ_k has been studied extensively in the delay embedding literature [46]. In this work we select a separate optimal τ_k for each subject and channel using the auto embedding method described in [48].

Indirect test of linearity. The results demonstrated in Figure 4 were obtained as follows. For each channel, we divided the iEEG dataset into 3 sub-datasets, with the first one including only STIM OFF data while the other 2 contained only STIM ON durations. Using the first dataset, we trained an AR model with parameter matrices $\{A_k^{(1)}\}$. The second dataset was used to learn an ARX model with parameter matrices $\{A_k^{(2)}\}$ and $\{B_k^{(2)}\}$. Finally, a second ARX model was trained on dataset 2 by fixing autoregressive weights to $\{A_k^{(1)}\}$ and only learning $\{B_k^{(3)}\}$. We then tested the two ARX models $\{A_k^{(1)}, B_k^{(3)}\}$ and $\{A_k^{(2)}, B_k^{(2)}\}$ on the third dataset. If the underlying process is indeed linear, we expect the autoregressive weights ($\{A_k\}$) to remain the same during STIM ON and STIM OFF durations, which would result in the ARX model $\{A_k^{(1)}, B_k^{(3)}\}$ performing as good as $\{A_k^{(2)}, B_k^{(2)}\}$. However, if the process is nonlinear, the latter would perform significantly better because of having both $\{A_k\}$ and $\{B_k\}$ trained on STIM ON data.

Bootstrap Test. For each subject and channel, we used a bootstrap test to validate if the presence of input lags significantly improved the prediction accuracy (i.e., whether a direct causal effect from input to that channel existed). From the original dataset $\mathcal{D} = \{Y_k, U_k, Y_{-k}, \Delta y_k\}$ for channel k (where Y_{-k} corresponds to the iEEG information from all channels other than k) we created a synthetic one $\tilde{\mathcal{D}} = \{Y_k, \tilde{U}_k, Y_{-k}, \Delta y_k\}$ by randomly shuffling the input history vector $U_k(.)$ across time samples (i.e, $\tilde{U}_k(i) = U_k(j)$ for some random j). We then split this dataset into training and test sets, learn a dynamical model, and compute the corresponding test MSE as before. We repeated this process 100 times and compared the test MSE of the unshuffled model to the distribution of test MSEs from shuffled models to compute a sample-based p-value. We reject the null hypothesis of no input effect (i.e., conclude that a direct causal effect from input to that channel existed) if $p < 0.05$.

In addition to input effects, we also validated the causal effects of network interactions in each subject-channel using a similar bootstrap test, wherein we generate synthetic datasets for each channel by randomly shuffling the iEEG past lags of other available channels. Specifically, a synthetic dataset $\tilde{\mathcal{D}} = \{Y_k, U_k, \tilde{Y}_{-k}, \Delta y_k\}$ was created by randomly shuffling the network information history vector $Y_{-k}(.)$ across time samples (i.e, $\tilde{Y}_{-k}(i) = Y_{-k}(j)$ for some random j). The test for network effects follows the same experimental structure as described in the previous paragraph.

Learning models on subsets of stimulation frequencies. The results reported in Figure 9 were generated as follows. We first split the dataset for each subject based on the stimulation frequency during each window and created multiple training sets corresponding to all subsets of $\{0, 10, 25, 50, 100, 200\}$. For each subset of frequencies, we fit a switched ARX model and tested it on the complementary subset of frequencies omitted in the training set. The normalized MSEs for all the combinations are reported in Figure 9.

Acknowledgements. The research performed in this study was supported in part by National Science Foundation Award Number 2239654.

Author Contributions. EN designed and supervised the study; GA performed the analyses; KAD co-supervised the selection and processing of the data and the empirical interpretation of the results; all authors wrote the manuscript.

Additional Information. Data availability: The iEEG data used in this study is publicly available from the RAM Public Data Release at `http://memory.psych.upenn.edu/RAM`.

Code availability: Python code for the analyses in this study is publicly available at

https://github.com/nozarilab/2023Acharya_evoked_ieeg.

References

[1] T. L. Skarpaas, B. Jarosiewicz, and M. J. Morrell, "Brain-responsive neurostimulation for epilepsy (rns® system)," *Epilepsy Research*, vol. 153, pp. 68–70, 2019.

[2] A. Schulze-Bonhage, "Principles of neurostimulation," in *Neurostimulation for Epilepsy*. Elsevier, 2023, pp. 1–29.

[3] V. Kokkinos, N. D. Sisterson, T. A. Wozny, and R. M. Richardson, "Association of closed-loop brain stimulation neurophysiological features with seizure control among patients with focal epilepsy," *JAMA neurology*, vol. 76, no. 7, pp. 800–808, 2019.

[4] G. K. Bergey, M. J. Morrell, E. M. Mizrahi, A. Goldman, D. King-Stephens, D. Nair, S. Srinivasan, B. Jobst, R. E. Gross, D. C. Shields *et al.*, "Long-term treatment with responsive brain stimulation in adults with refractory partial seizures," *Neurology*, vol. 84, no. 8, pp. 810–817, 2015.

[5] H. Kassiri, S. Tonekaboni, M. T. Salam, N. Soltani, K. Abdelhalim, J. L. P. Velazquez, and R. Genov, "Closed-loop neurostimulators: A survey and a seizure-predicting design example for intractable epilepsy treatment," *IEEE transactions on biomedical circuits and systems*, vol. 11, no. 5, pp. 1026–1040, 2017.

[6] D. R. Nair, K. D. Laxer, P. B. Weber, A. M. Murro, Y. D. Park, G. L. Barkley, B. J. Smith, R. P. Gwinn, M. J. Doherty, K. H. Noe *et al.*, "Nine-year prospective efficacy and safety of brain-responsive neurostimulation for focal epilepsy," *Neurology*, vol. 95, no. 9, pp. e1244–e1256, 2020.

[7] A. Li, C. Huynh, Z. Fitzgerald, I. Cajigas, D. Brusko, J. Jagid, A. O. Claudio, A. M. Kanner, J. Hopp, S. Chen *et al.*, "Neural fragility as an eeg marker of the seizure onset zone," *Nature neuroscience*, vol. 24, no. 10, pp. 1465–1474, 2021.

[8] A. Ashourvan, S. Pequito, A. N. Khambhati, F. Mikhail, S. N. Baldassano, K. A. Davis, T. H. Lucas, J. M. Vettel, B. Litt, G. J. Pappas, and D. S. Bassett, "Model-based design for seizure control by stimulation," *Journal of Neural Engineering*, vol. 17, no. 2, p. 026009, 2020.

[9] S. Chatterjee, O. Romero, A. Ashourvan, and S. D. G. M. Pequito, "Fractional-order model predictive control as a framework for electrical neurostimulation in epilepsy," *Journal of Neural Engineering*, 2020.

[10] G. Baier, M. Goodfellow, P. N. Taylor, Y. Wang, and D. J. Garry, "The importance of modeling epileptic seizure dynamics as spatio-temporal patterns," *Frontiers in physiology*, vol. 3, p. 281, 2012.

[11] D. Fan and Q. Wang, "Closed-loop control of absence seizures inspired by feedback modulation of basal ganglia to the corticothalamic circuit," *IEEE Transactions on Neural Systems and Rehabilitation Engineering*, vol. 28, no. 3, pp. 581–590, 2020.

[12] L. Xia, A. Soltan, X. Zhang, A. Jackson, R. Tessier, and P. Degenaar, "Closed-loop proportion-derivative control of suppressing seizures in a neural mass model," in *2019 IEEE International Symposium on Circuits and Systems (ISCAS)*. IEEE, 2019, pp. 1–5.

[13] T. Proix, V. K. Jirsa, F. Bartolomei, M. Guye, and W. Truccolo, "Predicting the spatiotemporal diversity of seizure propagation and termination in human focal epilepsy," *Nature communications*, vol. 9, no. 1, pp. 1–15, 2018.

[14] C.-S. Ouyang, R.-C. Yang, C.-T. Chiang, R.-C. Wu, and L.-C. Lin, "Eeg autoregressive modeling analysis: A diagnostic tool for patients with epilepsy without epileptiform discharges," *Clinical Neurophysiology*, vol. 131, no. 8, pp. 1902–1908, 2020.

[15] P.-N. Yu, S. A. Naiini, C. N. Heck, C. Y. Liu, D. Song, and T. W. Berger, "A sparse laguerre-volterra autoregressive model for seizure prediction in temporal lobe epilepsy," in *2016 38th Annual International Conference of the IEEE Engineering in Medicine and Biology Society (EMBC)*. IEEE, 2016, pp. 1664–1667.

[16] D. Rafik and B. Larbi, "Autoregressive modeling based empirical mode decomposition (EMD) for epileptic seizures detection using EEG signals," 2019.

[17] L. Chisci, A. Mavino, G. Perferi, M. Sciandrone, C. Anile, G. Colicchio, and F. Fuggetta, "Real-time epileptic seizure prediction using ar models

and support vector machines," *IEEE Transactions on Biomedical Engineering*, vol. 57, no. 5, pp. 1124–1132, 2010.

[18] A. Attia, A. Moussaoui, and Y. Chahir, "Epileptic seizures identification with autoregressive model and firefly optimization based classification," *Evolving Systems*, pp. 1–10, 2019.

[19] A. Aarabi and B. He, "Seizure prediction in hippocampal and neocortical epilepsy using a model-based approach," *Clinical Neurophysiology*, vol. 125, no. 5, pp. 930–940, 2014.

[20] G. Wang, Z. Sun, R. Tao, K. Li, G. Bao, and X. Yan, "Epileptic seizure detection based on partial directed coherence analysis," *IEEE journal of biomedical and health informatics*, vol. 20, no. 3, pp. 873–879, 2015.

[21] A. Alkan and M. K. Kiymik, "Comparison of ar and welch methods in epileptic seizure detection," *Journal of Medical Systems*, vol. 30, no. 6, pp. 413–419, 2006.

[22] Z. Rogowski, I. Gath, and E. Bental, "On the prediction of epileptic seizures," *Biological cybernetics*, vol. 42, no. 1, pp. 9–15, 1981.

[23] A. Li, S. Inati, K. Zaghloul, and S. Sarma, "Fragility in epileptic networks: the epileptogenic zone," in *2017 American Control Conference (ACC)*. IEEE, 2017, pp. 2817–2822.

[24] C. J. Anderson, D. N. Anderson, S. M. Pulst, C. R. Butson, and A. D. Dorval, "Neural selectivity, efficiency, and dose equivalence in deep brain stimulation through pulse width tuning and segmented electrodes," *Brain Stimulation*, 2020.

[25] M. Keane, S. Deyo, A. Abosch, J. A. Bajwa, and M. D. Johnson, "Improved spatial targeting with directionally segmented deep brain stimulation leads for treating essential tremor," *Journal of neural engineering*, vol. 9, no. 4, p. 046005, 2012.

[26] J. Buhlmann, L. Hofmann, P. A. Tass, and C. Hauptmann, "Modeling of a segmented electrode for desynchronizing deep brain stimulation," *Frontiers in neuroengineering*, vol. 4, p. 15, 2011.

[27] L. M. Zitella, K. Mohsenian, M. Pahwa, C. Gloeckner, and M. D. Johnson, "Computational modeling of pedunculopontine nucleus deep brain stimulation," *Journal of neural engineering*, vol. 10, no. 4, p. 045005, 2013.

[28] C. Liu, J. Wang, H. Li, M. Lu, B. Deng, H. Yu, X. Wei, C. Fietkiewicz, and K. A. Loparo, "Closed-loop modulation of the pathological disorders of the basal ganglia network," *IEEE Transactions on Neural Networks and Learning Systems*, vol. 28, no. 2, pp. 371–382, 2016.

[29] C.-F. Wang, S.-H. Yang, S.-H. Lin, P.-C. Chen, Y.-C. Lo, H.-C. Pan, H.-Y. Lai, L.-D. Liao, H.-C. Lin, H.-Y. Chen *et al.*, "A proof-of-principle simulation for closed-loop control based on preexisting experimental thalamic dbs-enhanced instrumental learning," *Brain Stimulation*, vol. 10, no. 3, pp. 672–683, 2017.

[30] G. Pedoto, S. Santaniello, E. B. Montgomery, J. T. Gale, G. Fiengo, L. Glielmo, and S. V. Sarma, "System identification of local field potentials under deep brain stimulation in a healthy primate," in *2010 Annual International Conference of the IEEE Engineering in Medicine and Biology*. IEEE, 2010, pp. 4144–4147.

[31] S. Santaniello, G. Fiengo, L. Glielmo, and W. M. Grill, "Closed-loop control of deep brain stimulation: a simulation study," *IEEE Transactions on Neural Systems and Rehabilitation Engineering*, vol. 19, no. 1, pp. 15–24, 2010.

[32] S. Chang, X. Wei, F. Su, C. Liu, G. Yi, J. Wang, C. Han, and Y. Che, "Model predictive control for seizure suppression based on nonlinear auto-regressive moving-average volterra model," *IEEE Transactions on Neural Systems and Rehabilitation Engineering*, vol. 28, no. 10, pp. 2173–2183, 2020.

[33] F. Su, J. Wang, S. Niu, H. Li, B. Deng, C. Liu, and X. Wei, "Nonlinear predictive control for adaptive adjustments of deep brain stimulation parameters in basal ganglia–thalamic network," *Neural Networks*, vol. 98, pp. 283–295, 2018.

[34] Y. Yang, S. Qiao, O. G. Sani, J. I. Sedillo, B. Ferrentino, B. Pesaran, and M. M. Shanechi, "Modelling and prediction of the dynamic responses of large-scale brain networks during direct electrical stimulation," *Nature biomedical engineering*, vol. 5, no. 4, pp. 324–345, 2021.

[35] J.-Y. Chang, A. Pigorini, M. Massimini, G. Tononi, L. Nobili, and B. D. Van Veen, "Multivariate autoregressive models with exogenous inputs for intracerebral responses to direct electrical stimulation of the human brain," *Frontiers in human neuroscience*, vol. 6, p. 317, 2012.

[36] U. R. Mohan, A. J. Watrous, J. F. Miller, B. C. Lega, M. R. Sperling, G. A. Worrell, R. E. Gross, K. A. Zaghloul, B. C. Jobst, K. A. Davis *et al.*, "The effects of direct brain stimulation in humans depend on frequency, amplitude, and white-matter proximity," *Brain stimulation*, vol. 13, no. 5, pp. 1183–1195, 2020.

[37] L. Ljung, "System identification: theory for the user," *PTR Prentice Hall, Upper Saddle River, NJ*, pp. 1–14, 1999.

[38] G. Acharya, S. F. Ruf, and E. Nozari, "Brain modeling for control: A review," *Frontiers in Control Engineering*, vol. 3, Dec. 2022. [Online]. Available: https://doi.org/10.3389/fcteg.2022.1046764

[39] E. Nozari, J. Stiso, L. Caciagli, E. J. Cornblath, X. He, M. A. Bertolero, A. S. Mahadevan, G. J. Pappas, and D. S. Bassett, "Is the brain macroscopically linear? a system identification of resting state dynamics," *Nature Biomedical Engineering*, 2023, in press, available at https://www.biorxiv.org/content/early/2020/12/22/2020.12.21.423856.

[40] A. Haddock, A. Velisar, J. Herron, H. Bronte-Stewart, and H. J. Chizeck, "Model predictive control of deep brain stimulation for parkinsonian tremor," in *2017 8th International IEEE/EMBS Conference on Neural Engineering (NER)*. IEEE, 2017, pp. 358–362.

[41] J. Kahan, L. Mancini, G. Flandin, M. White, A. Papadaki, J. Thornton, T. Yousry, L. Zrinzo, M. Hariz, P. Limousin *et al.*, "Deep brain stimulation has state-dependent effects on motor connectivity in parkinson's disease," *Brain*, vol. 142, no. 8, pp. 2417–2431, 2019.

[42] C. Steinhardt, P. Sacré, T. Sheehan, J. Wittig, Jr, S. Inati, S. Sarma, and K. Zaghloul, "Characterizing and predicting cortical evoked responses to direct electrical stimulation of the human brain," *Brain Stimulation*, vol. 13, 06 2020.

[43] J. Durbin and S. J. Koopman, *Time series analysis by state space methods*. OUP Oxford, 2012, vol. 38.

[44] L. E. Baum and T. Petrie, "Statistical inference for probabilistic functions of finite state markov chains," *The annals of mathematical statistics*, vol. 37, no. 6, pp. 1554–1563, 1966.

[45] C. W. Granger, "Investigating causal relations by econometric models and cross-spectral methods," *Econometrica: journal of the Econometric Society*, pp. 424–438, 1969.

[46] L. Noakes, "The takens embedding theorem," *International Journal of Bifurcation and Chaos*, vol. 1, no. 04, pp. 867–872, 1991.

[47] J. Huke, "Embedding nonlinear dynamical systems: A guide to takens' theorem," 2006.

[48] M. Otani and A. Jones, "Automated embedding and creepphenomenon in chaotic time series," 2000.

[49] P. Faure and H. Korn, "Is there chaos in the brain? i. concepts of nonlinear dynamics and methods of investigation," *Comptes Rendus de l'Académie des Sciences-Series III-Sciences de la Vie*, vol. 324, no. 9, pp. 773–793, 2001.

[50] K.-R. Muller, C. W. Anderson, and G. E. Birch, "Linear and nonlinear methods for brain-computer interfaces," *IEEE transactions on neural systems and rehabilitation engineering*, vol. 11, no. 2, pp. 165–169, 2003.

[51] D. Liberzon, *Switching in Systems and Control*, ser. Systems & Control: Foundations & Applications. Birkhäuser Boston, 2003.

[52] J. Pearl, "The do-calculus revisited," *arXiv preprint arXiv:1210.4852*, 2012.

[53] S. S. Balaji and K. K. Parhi, "Seizure onset zone identification from ieeg: A review," *IEEE Access*, vol. 10, pp. 62 535–62 547, 2022.

[54] A. N. Khambhati, D. S. Bassett, B. S. Oommen, S. H. Chen, T. H. Lucas, K. A. Davis, and B. Litt, "Recurring functional interactions predict network architecture of interictal and ictal states in neocortical epilepsy," *eneuro*, vol. 4, no. 1, 2017.

[55] F. T. Sun and M. J. Morrell, "Closed-loop neurostimulation: the clinical experience," *Neurotherapeutics*, vol. 11, no. 3, pp. 553–563, 2014.

[56] I. Iturrate, M. Pereira, and J. d. R. Millán, "Closed-loop electrical neurostimulation: challenges and opportunities," *Current Opinion in Biomedical Engineering*, vol. 8, pp. 28–37, 2018.

[57] S. Ramgopal, S. Thome-Souza, M. Jackson, N. E. Kadish, I. S. Fernández, J. Klehm, W. Bosl, C. Reinsberger, S. Schachter, and

T. Loddenkemper, "Seizure detection, seizure prediction, and closed-loop warning systems in epilepsy," *Epilepsy & behavior*, vol. 37, pp. 291–307, 2014.

[58] A. Y. Kaplan, A. A. Fingelkurts, A. A. Fingelkurts, S. V. Borisov, and B. S. Darkhovsky, "Nonstationary nature of the brain activity as revealed by eeg/meg: methodological, practical and conceptual challenges," *Signal processing*, vol. 85, no. 11, pp. 2190–2212, 2005.

[59] L. D. Iasemidis, D.-S. Shiau, W. Chaovalitwongse, J. C. Sackellares, P. M. Pardalos, J. C. Principe, P. R. Carney, A. Prasad, B. Veeramani, and K. Tsakalis, "Adaptive epileptic seizure prediction system," *IEEE transactions on biomedical engineering*, vol. 50, no. 5, pp. 616–627, 2003.

[60] P. Kahane and A. Depaulis, "Deep brain stimulation in epilepsy: what is next?" *Current opinion in neurology*, vol. 23, no. 2, pp. 177–182, 2010.

[61] K. J. Friston, L. Harrison, and W. Penny, "Dynamic causal modelling," *Neuroimage*, vol. 19, no. 4, pp. 1273–1302, 2003.

[62] B. C. van Wijk, H. Cagnan, V. Litvak, A. A. Kühn, and K. J. Friston, "Generic dynamic causal modelling: An illustrative application to parkinson's disease," *NeuroImage*, vol. 181, pp. 818–830, 2018.

[63] K. J. Friston, "Variational filtering," *NeuroImage*, vol. 41, no. 3, pp. 747–766, 2008.

[64] S. J. Kiebel, M. I. Garrido, R. J. Moran, and K. J. Friston, "Dynamic causal modelling for eeg and meg," *Cognitive neurodynamics*, vol. 2, pp. 121–136, 2008.

[65] "Ram - computational memory lab," https://memory.psych.upenn.edu/RAM, [Accessed 14-Jul-2023].

[66] J. Birjandtalab, V. N. Jarmale, M. Nourani, and J. Harvey, "Impact of personalization on epileptic seizure prediction," in *2019 IEEE EMBS International Conference on Biomedical & Health Informatics (BHI)*. IEEE, 2019, pp. 1–4.

[67] "What are nonlinear arx models?" https://www.mathworks.com/help/ident/ug/what-are-nonlinear-arx-models.html#br7waeg, [Accessed 14-Jul-2023].

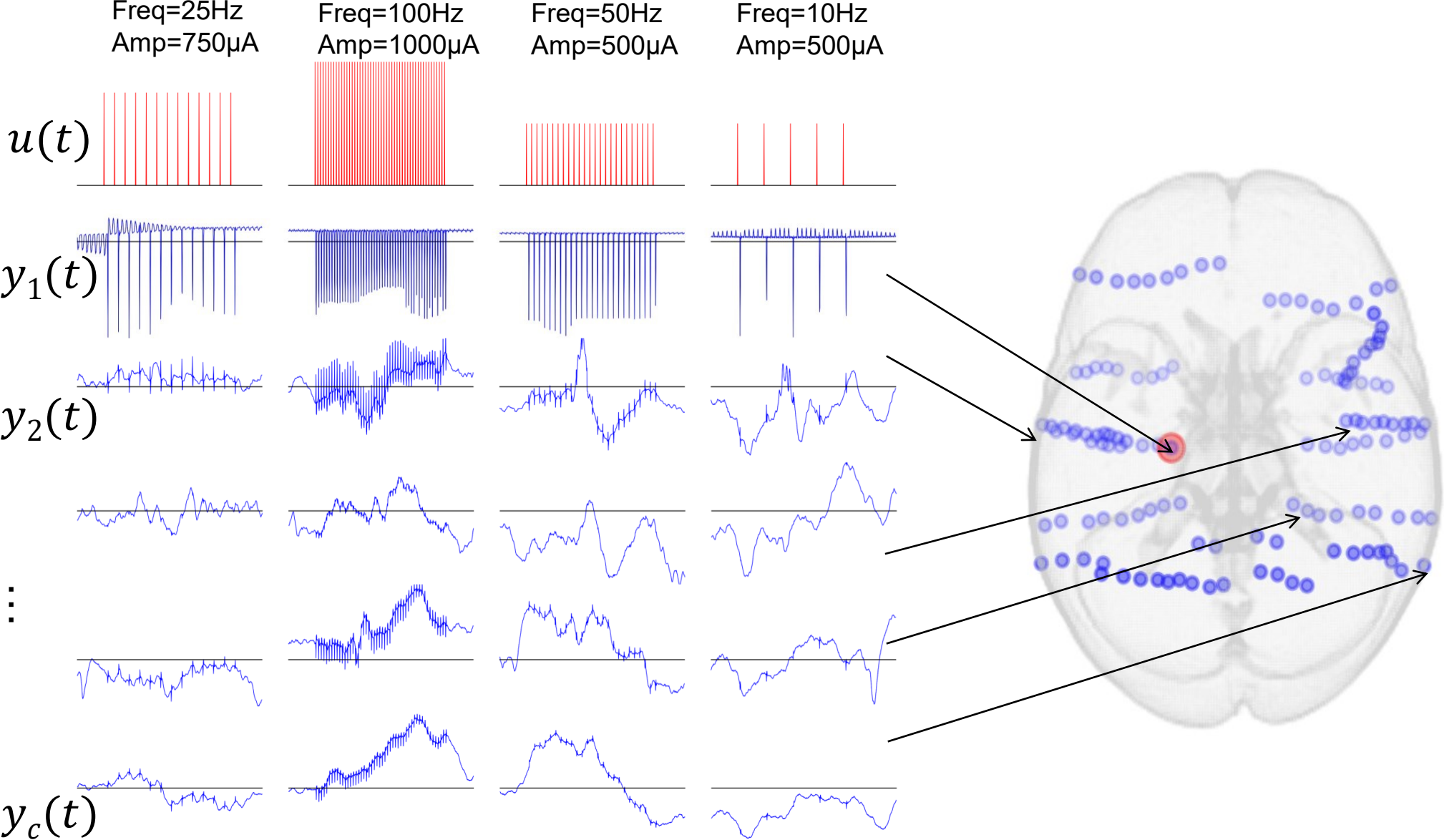
Freq=25Hz
Amp=750μA
Freq=100Hz
Amp=1000μA
Freq=50Hz
Amp=500μA
Freq=10Hz
Amp=500μA
$u(t)$
$y_1(t)$
$y_2(t)$
⋮
$y_c(t)$

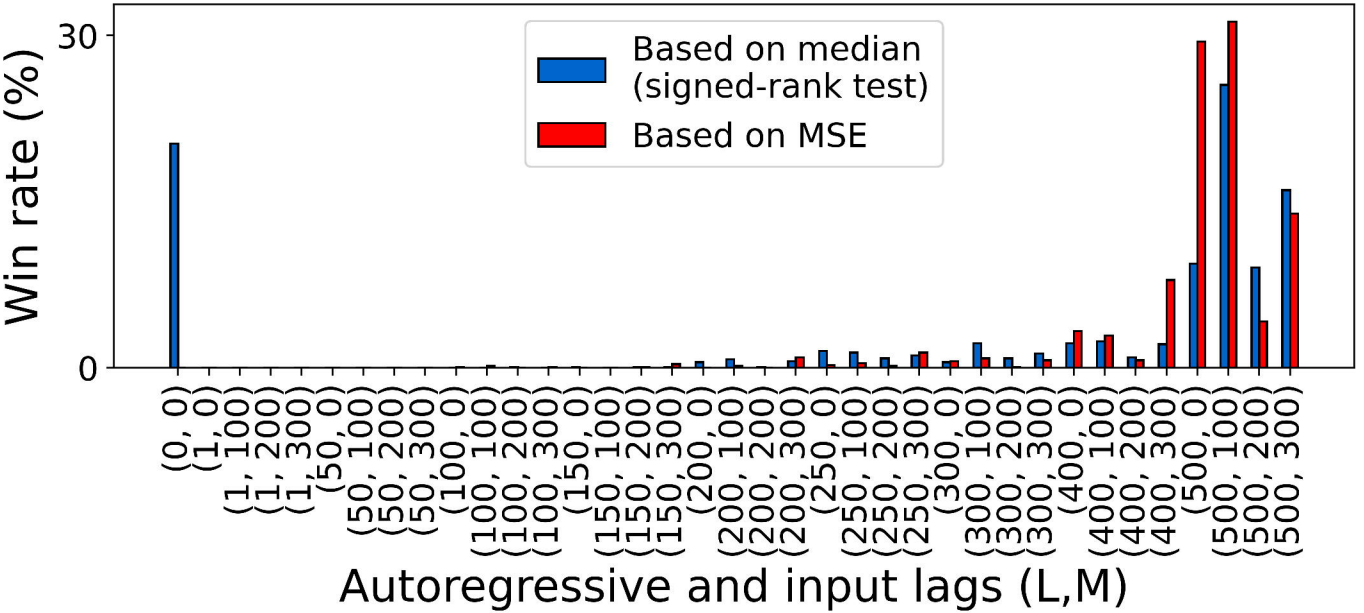
Based on median
(signed-rank test)
Based on MSE
Win rate (%)
30
0
(0, 0)
(1, 0)
(1, 100)
(1, 200)
(1, 300)
(50, 0)
(50, 100)
(50, 200)
(50, 300)
(100, 0)
(100, 100)
(100, 200)
(100, 300)
(150, 0)
(150, 100)
(150, 200)
(150, 300)
(200, 0)
(200, 100)
(200, 200)
(200, 300)
(250, 0)
(250, 100)
(250, 200)
(250, 300)
(300, 0)
(300, 100)
(300, 200)
(300, 300)
(400, 0)
(400, 100)
(400, 200)
(400, 300)
(500, 0)
(500, 100)
(500, 200)
(500, 300)
Autoregressive and input lags (L,M)

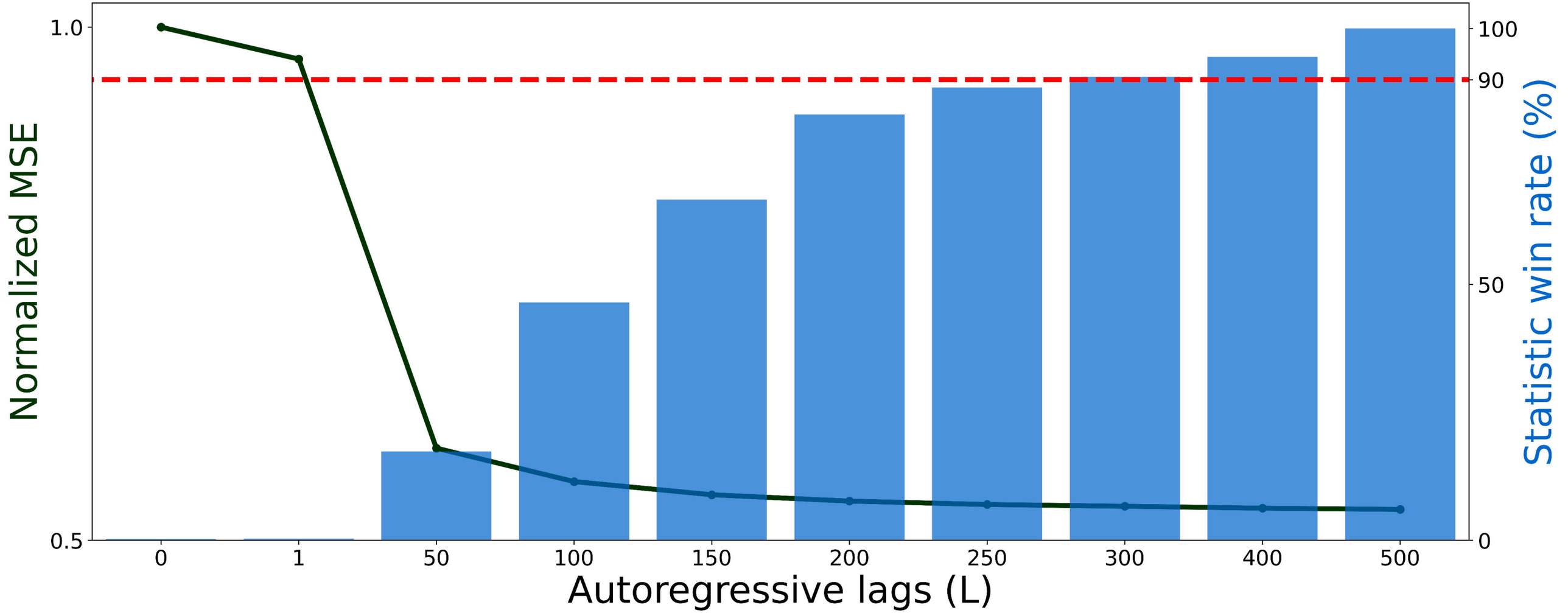
1.0
0.5
Normalized MSE
100
90
50
0
Statistic win rate (%)
0
1
50
100
150
200
250
300
400
500
Autoregressive lags (L)

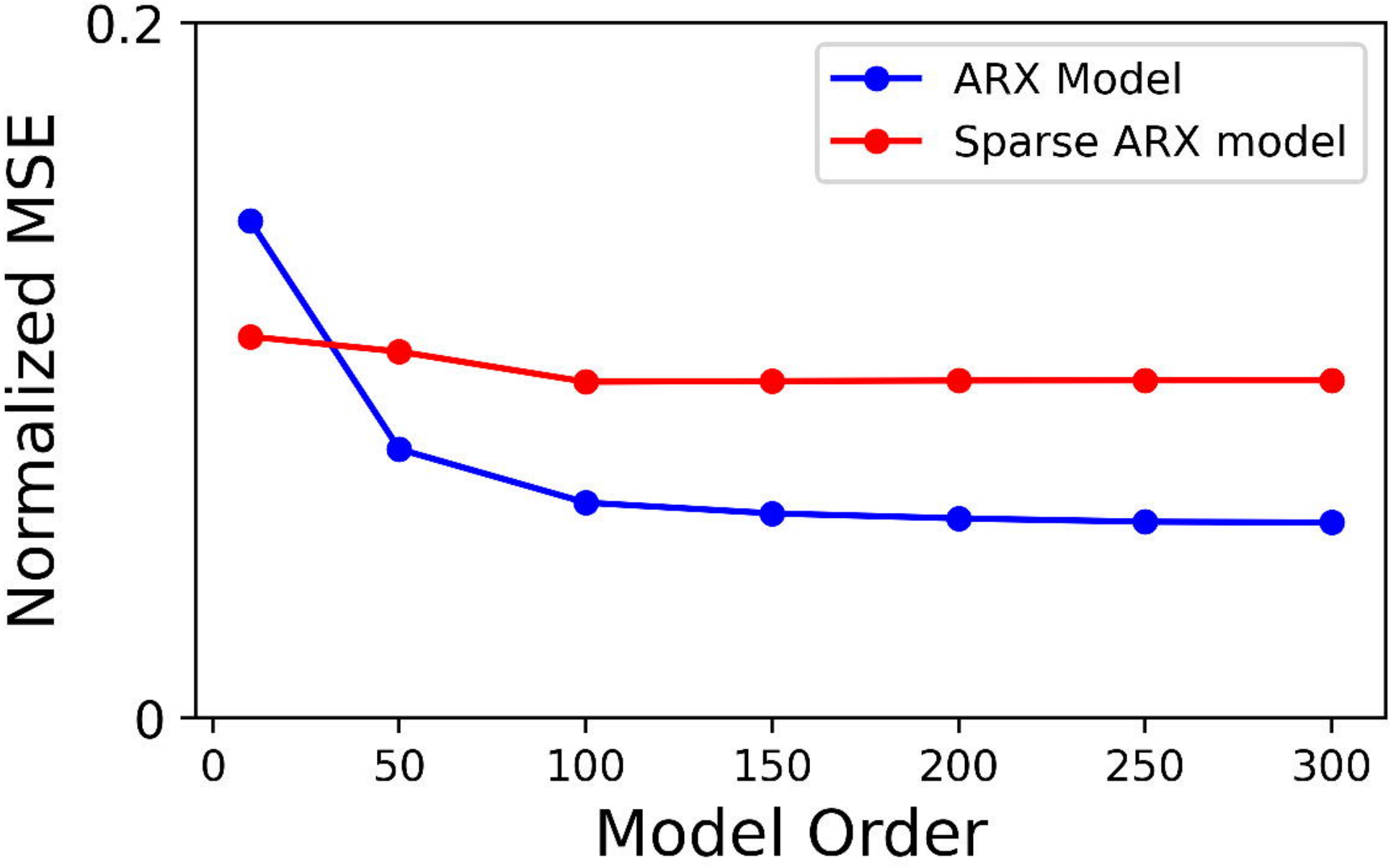
0.2
0
Normalized MSE
ARX Model
Sparse ARX model
0
50
100
150
200
250
300
Model Order

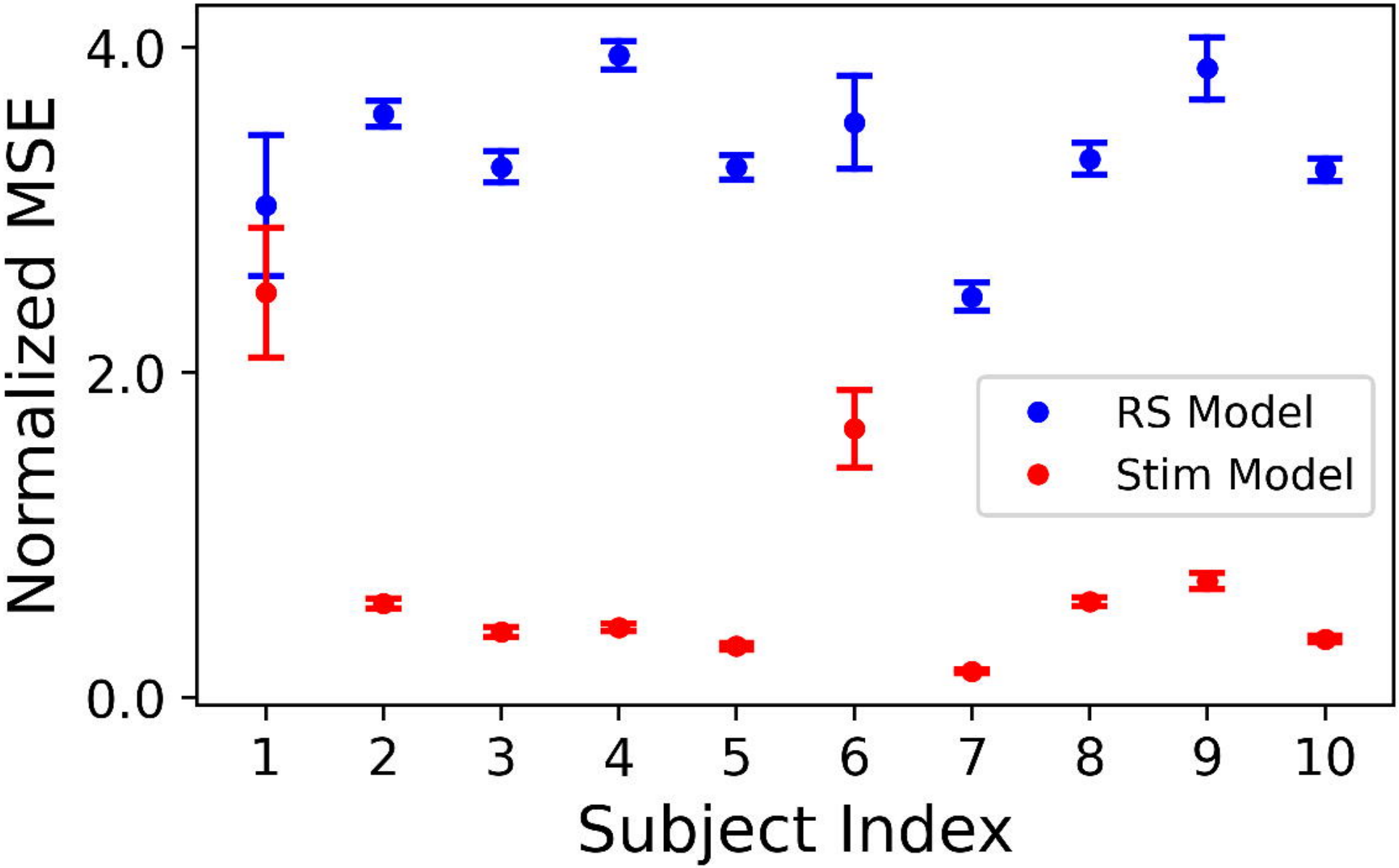
4.0
2.0
0.0
Normalized MSE
1
2
3
4
5
6
7
8
9
10
Subject Index
RS Model
Stim Model

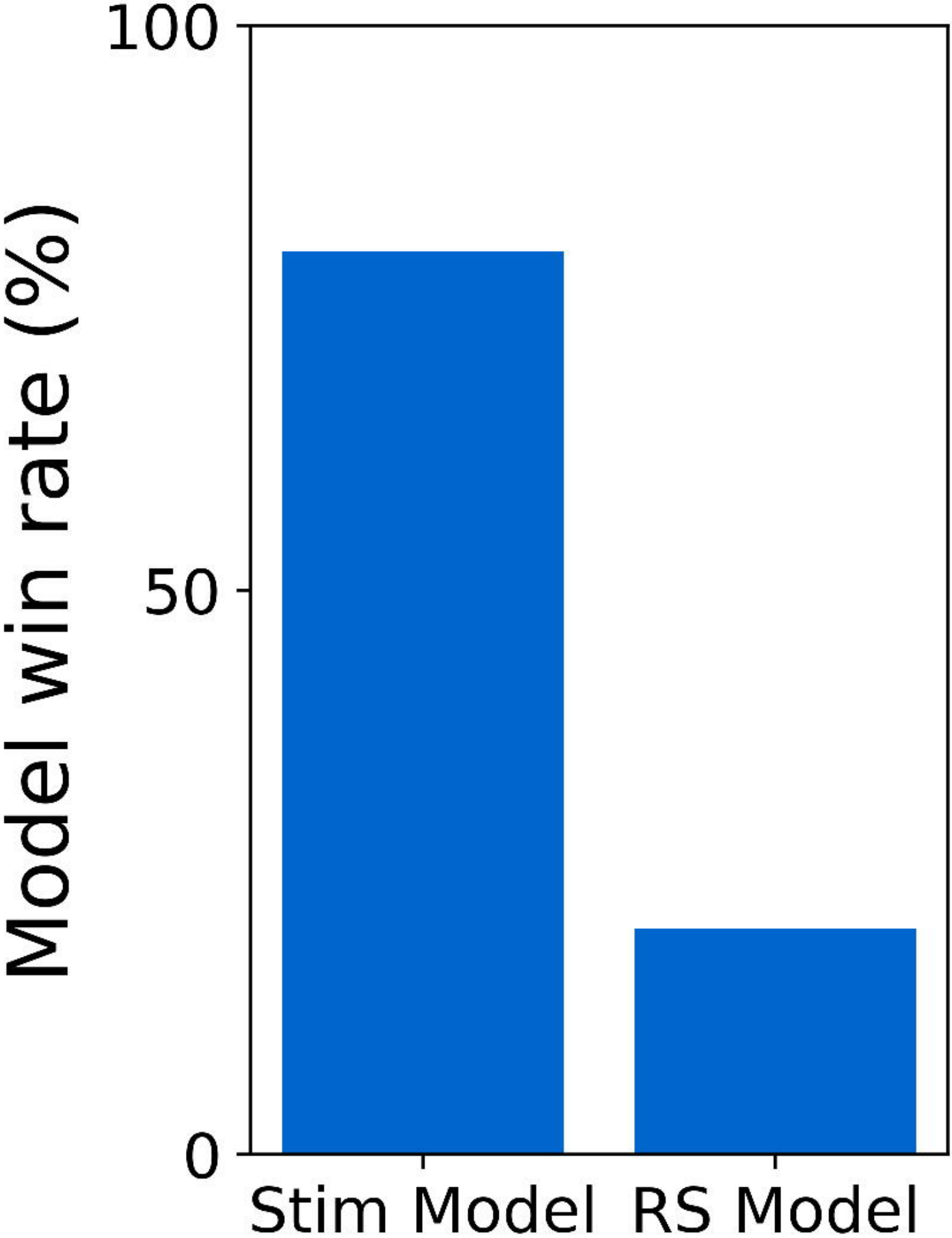
100
50
0
Model win rate (%)
Stim Model
RS Model

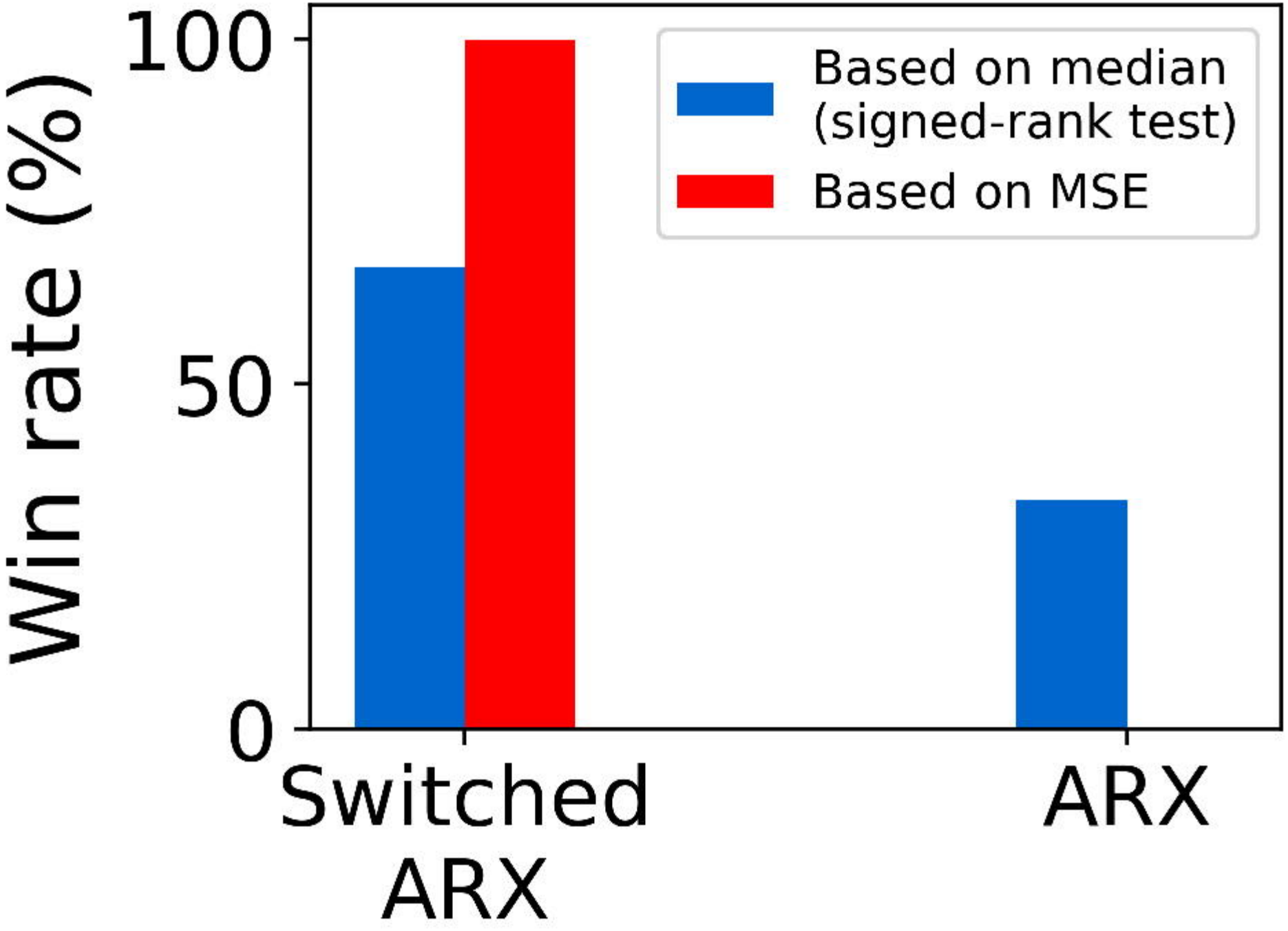
Win rate (%)
100
50
0
Based on median
(signed-rank test)
Based on MSE
Switched
ARX
ARX

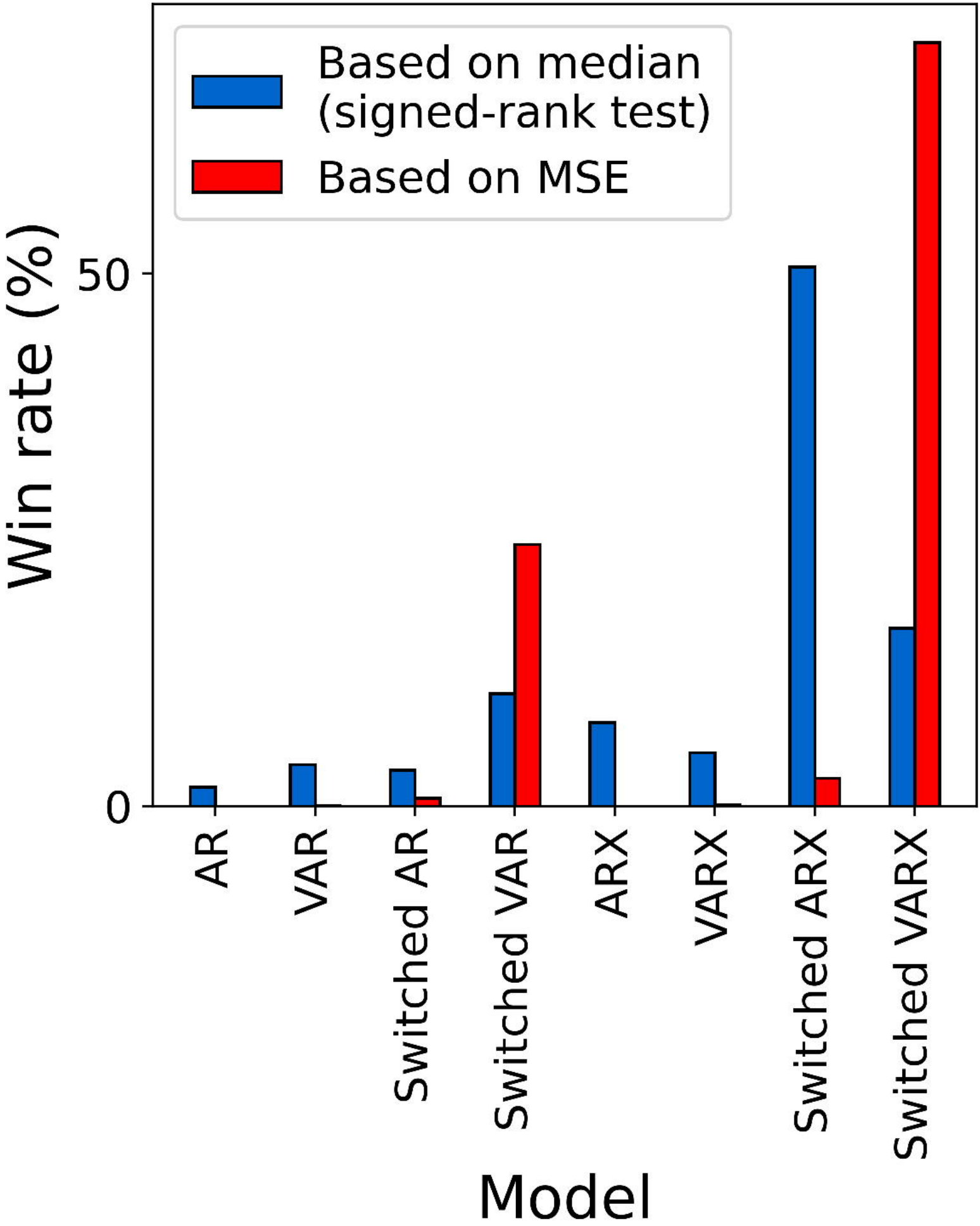
Based on median
(signed-rank test)
Based on MSE
Win rate (%)
50
0
AR
VAR
Switched AR
Switched VAR
ARX
VARX
Switched ARX
Switched VARX
Model

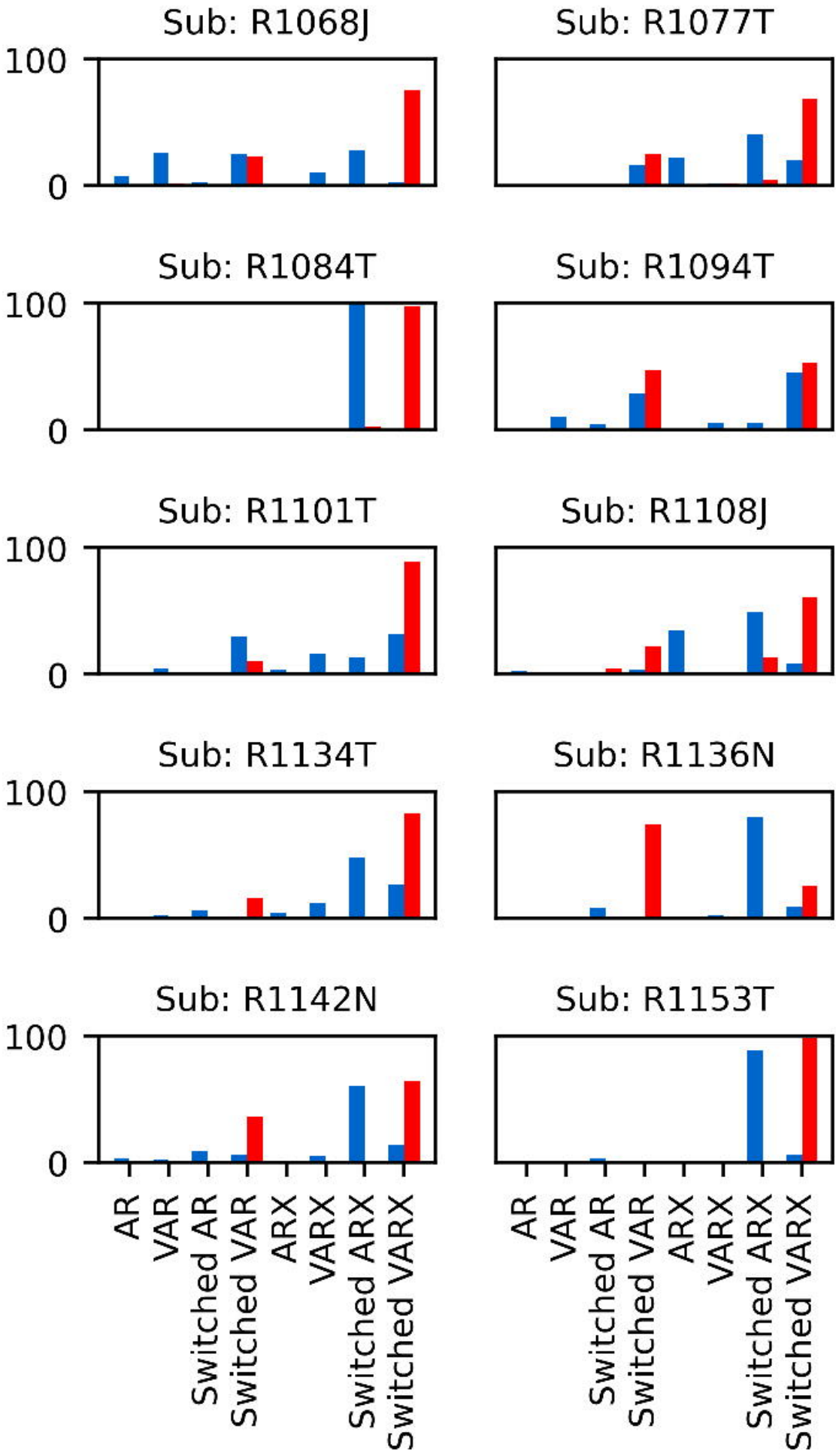
Sub: R1068J
Sub: R1077T
Sub: R1084T
Sub: R1094T
Sub: R1101T
Sub: R1108J
Sub: R1134T
Sub: R1136N
Sub: R1142N
Sub: R1153T
100
0
AR
VAR
Switched AR
Switched VAR
ARX
VARX
Switched ARX
Switched VARX

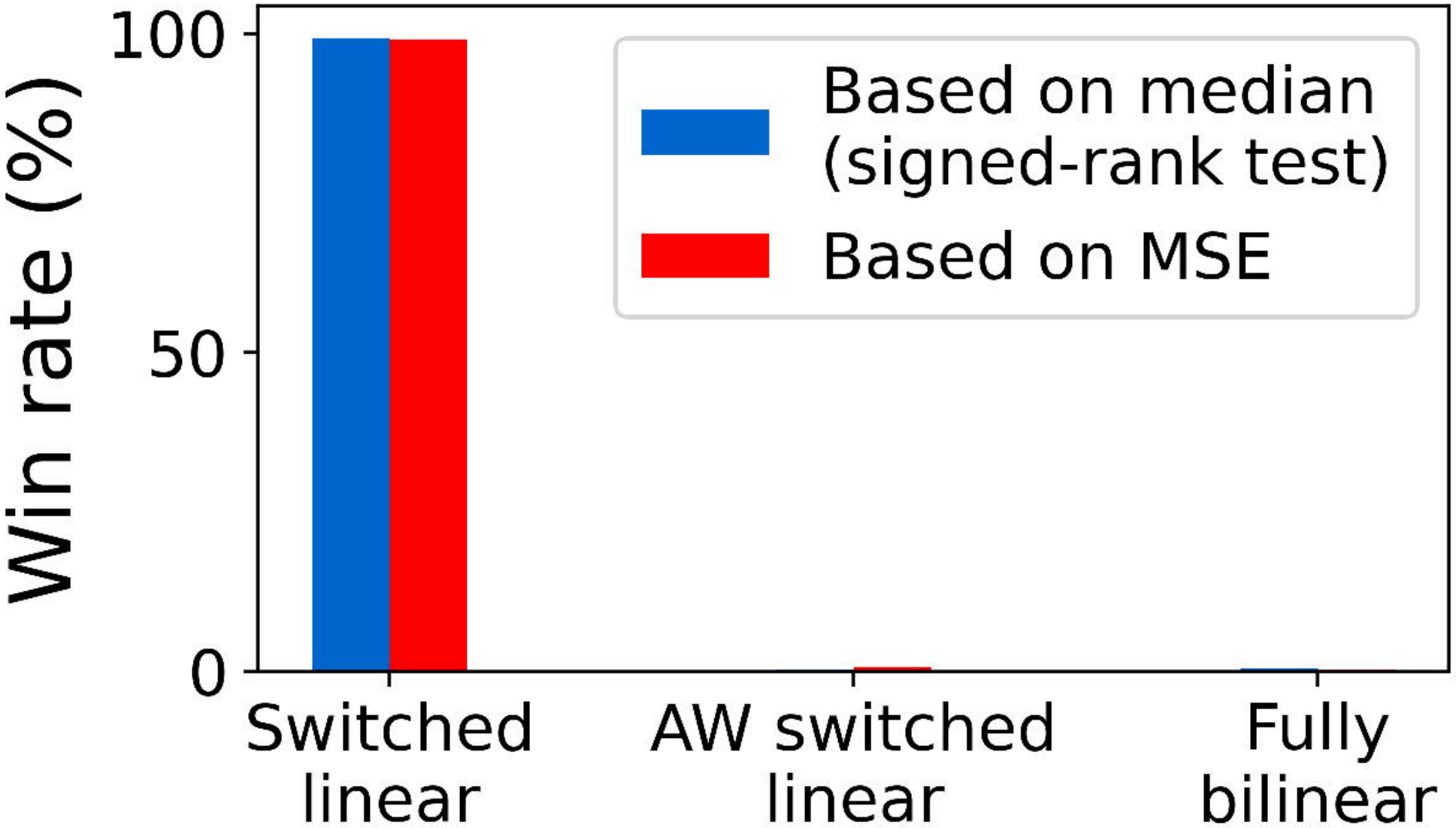
Win rate (%)
100
50
0
Based on median
(signed-rank test)
Based on MSE
Switched
linear
AW switched
linear
Fully
bilinear

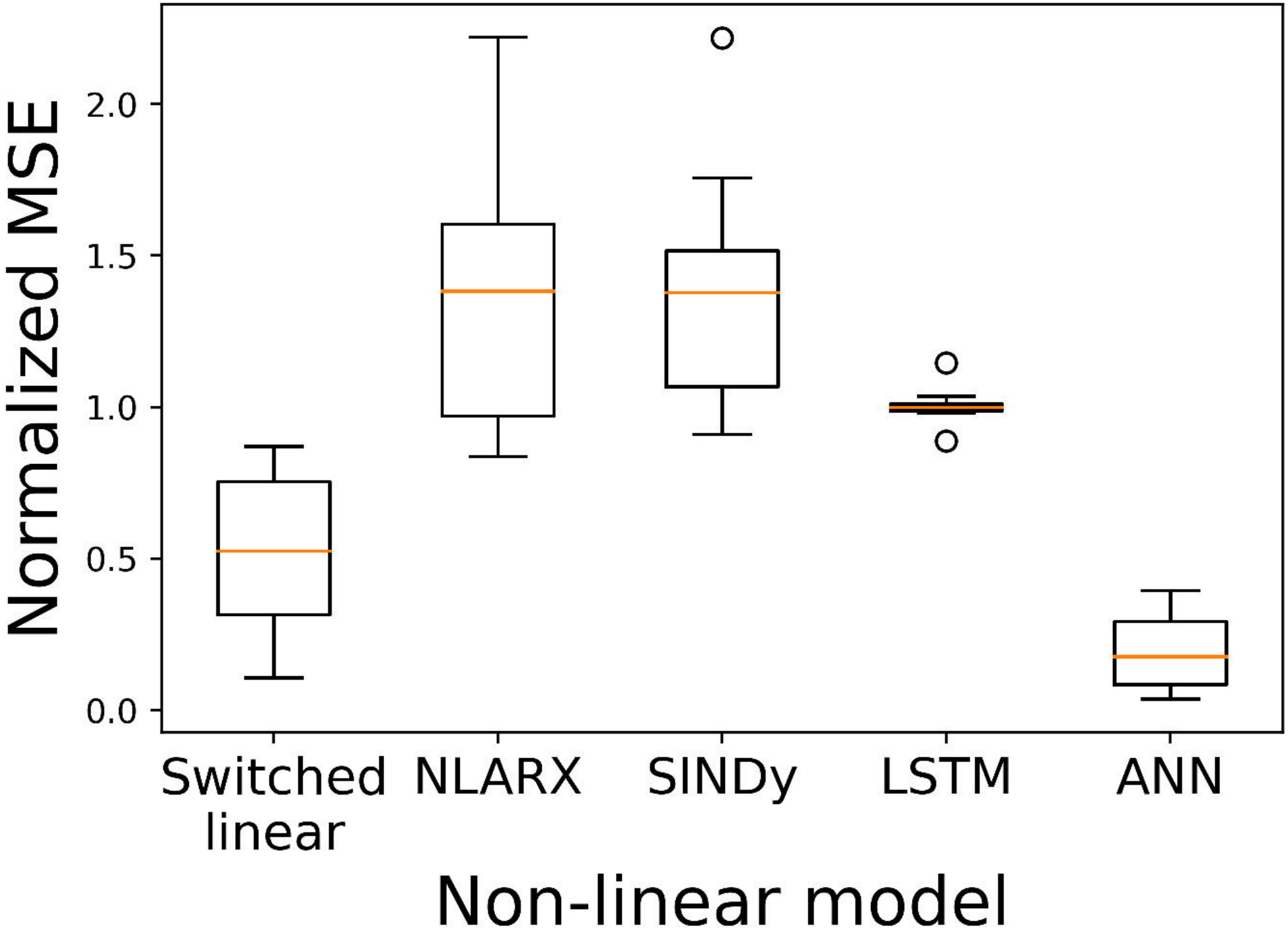
Normalized MSE
2.0
1.5
1.0
0.5
0.0
Switched linear
NLARX
SINDy
LSTM
ANN
Non-linear model

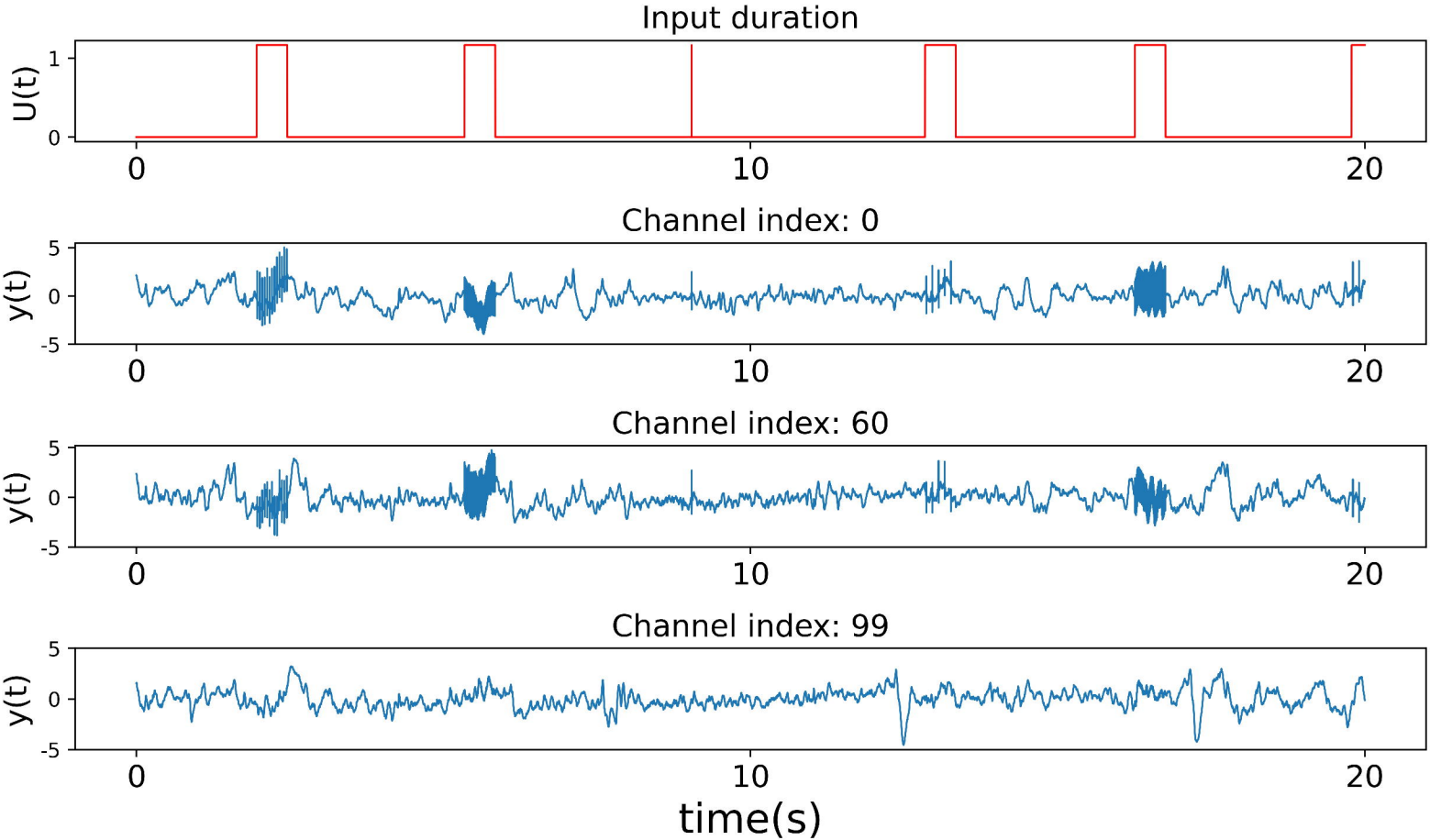
Input duration
U(t)
1
0
0
10
20
Channel index: 0
y(t)
5
0
-5
0
10
20
Channel index: 60
y(t)
5
0
-5
0
10
20
Channel index: 99
y(t)
5
0
-5
0
10
20
time(s)

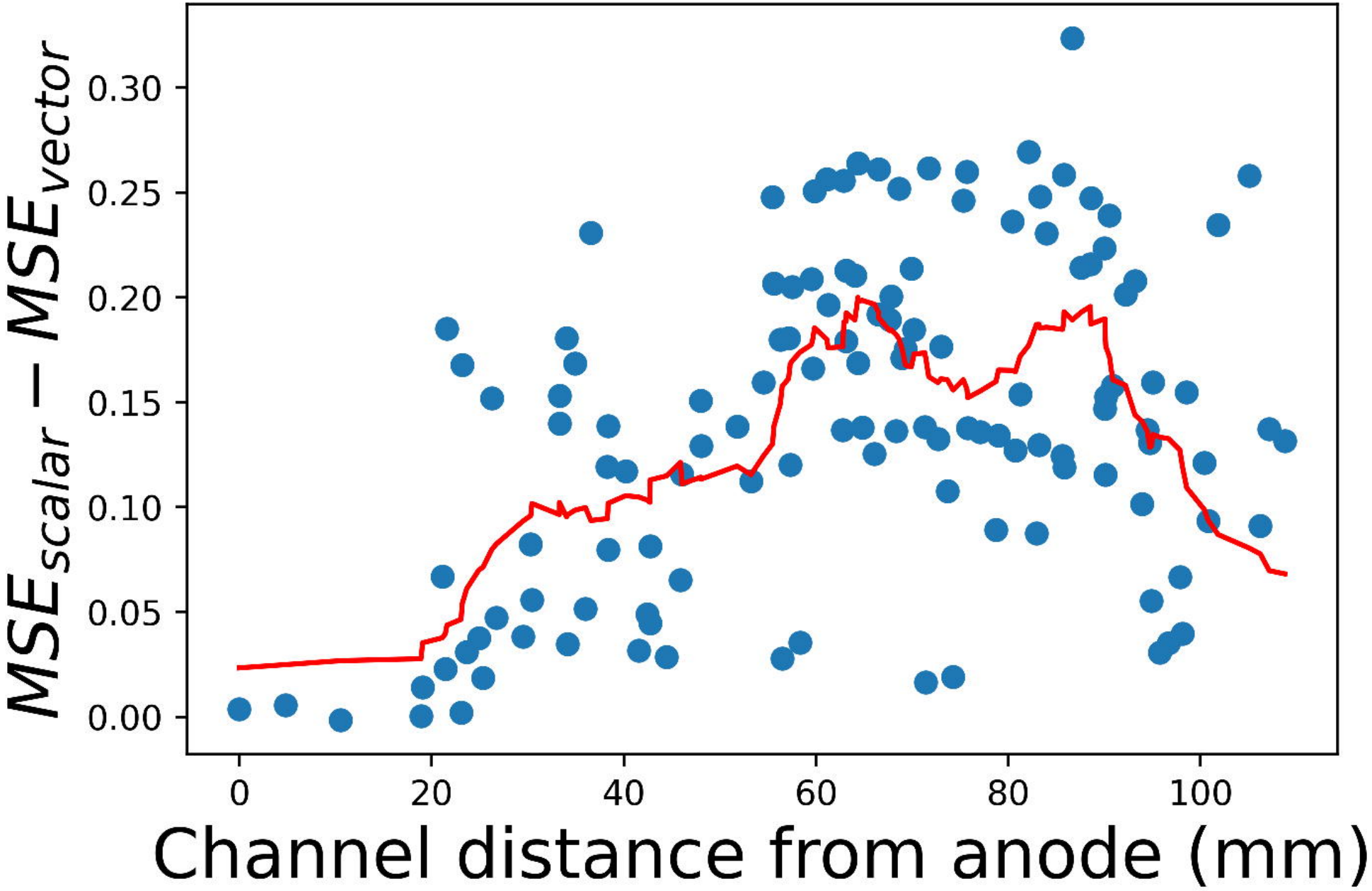
$MSE_{scalar} - MSE_{vector}$
0.30
0.25
0.20
0.15
0.10
0.05
0.00
0
20
40
60
80
100
Channel distance from anode (mm)

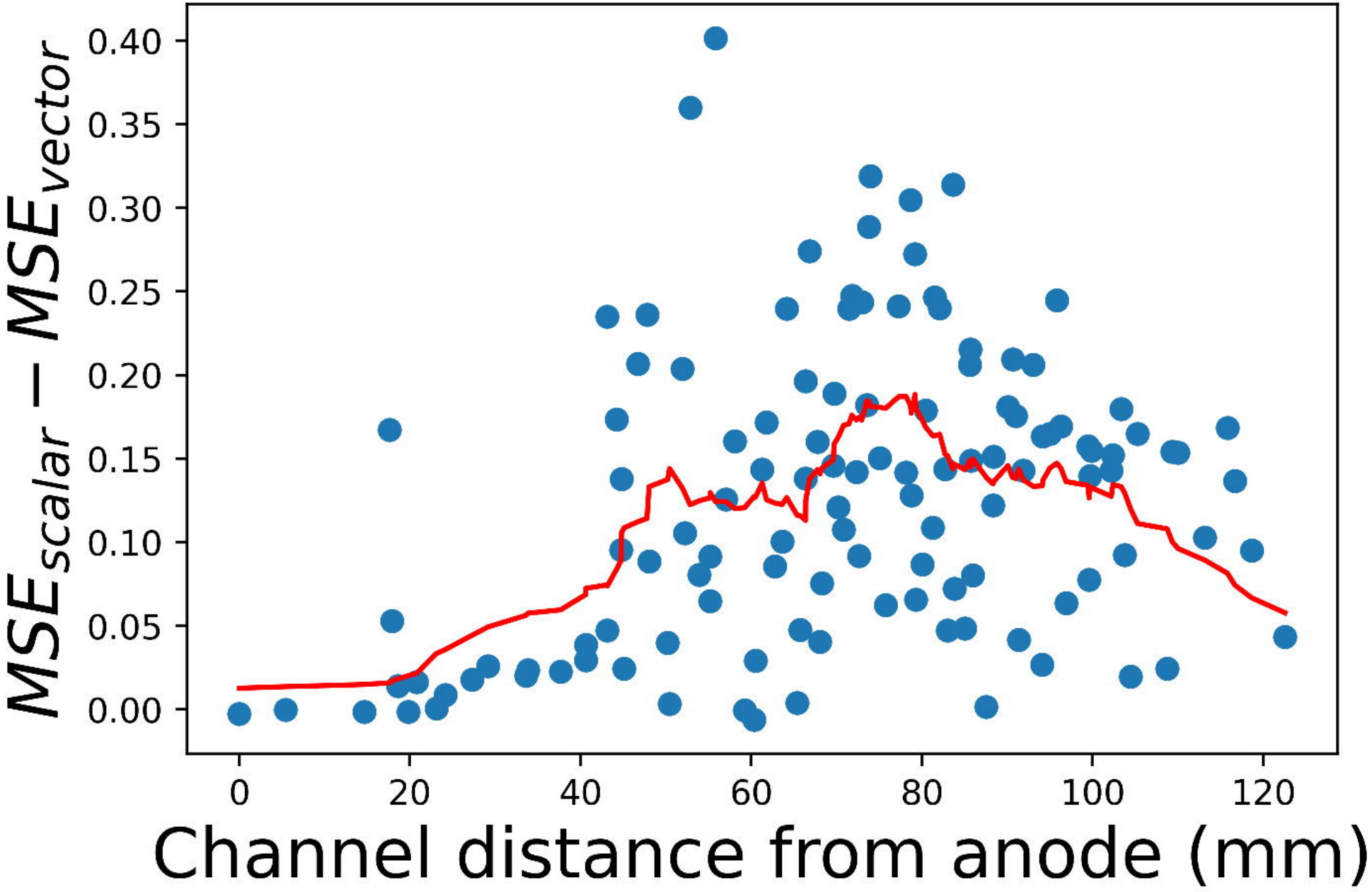
$MSE_{scalar} - MSE_{vector}$
0.40
0.35
0.30
0.25
0.20
0.15
0.10
0.05
0.00
0
20
40
60
80
100
120
Channel distance from anode (mm)

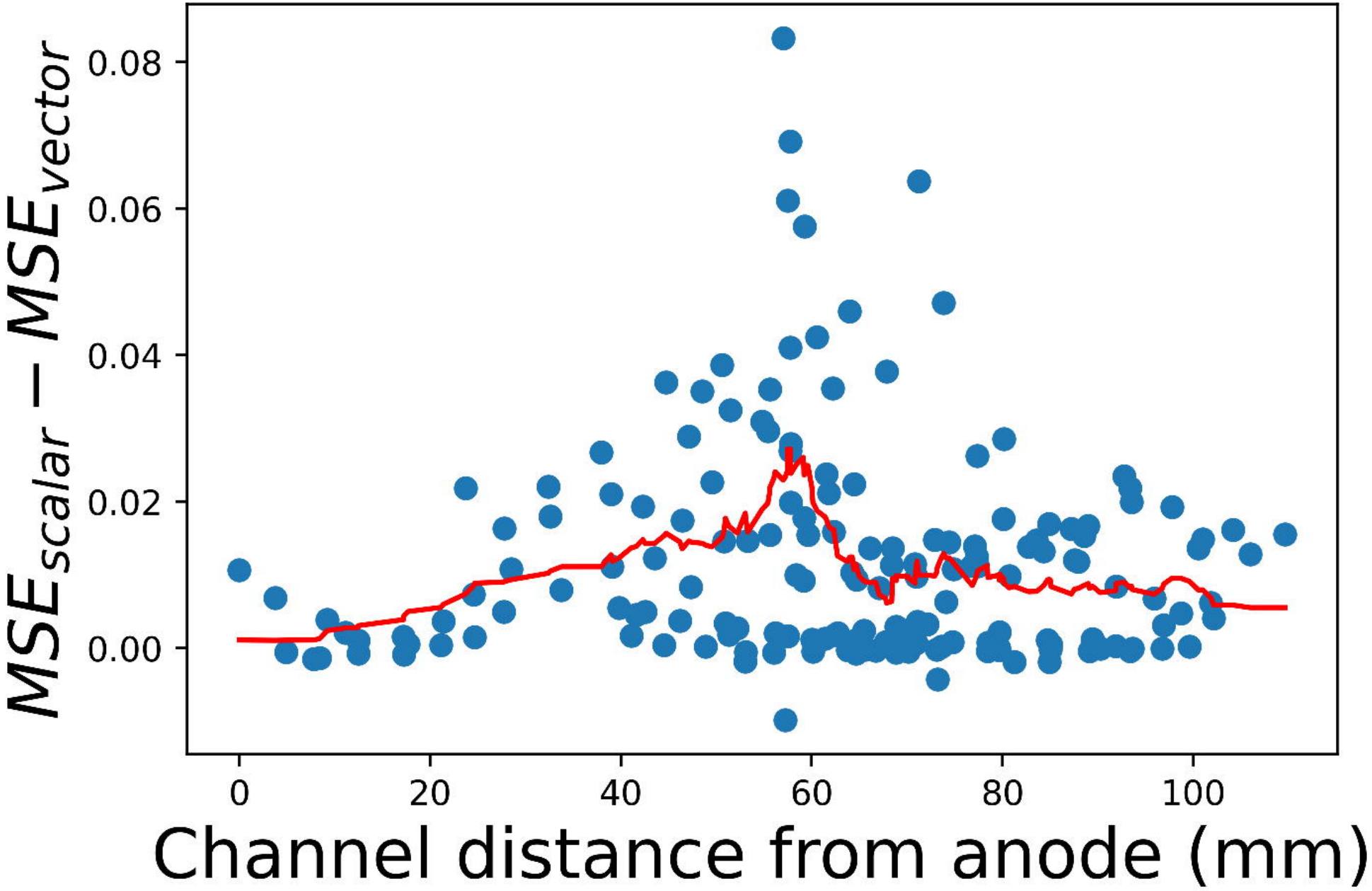
$MSE_{scalar} - MSE_{vector}$
0.08
0.06
0.04
0.02
0.00
0
20
40
60
80
100
Channel distance from anode (mm)

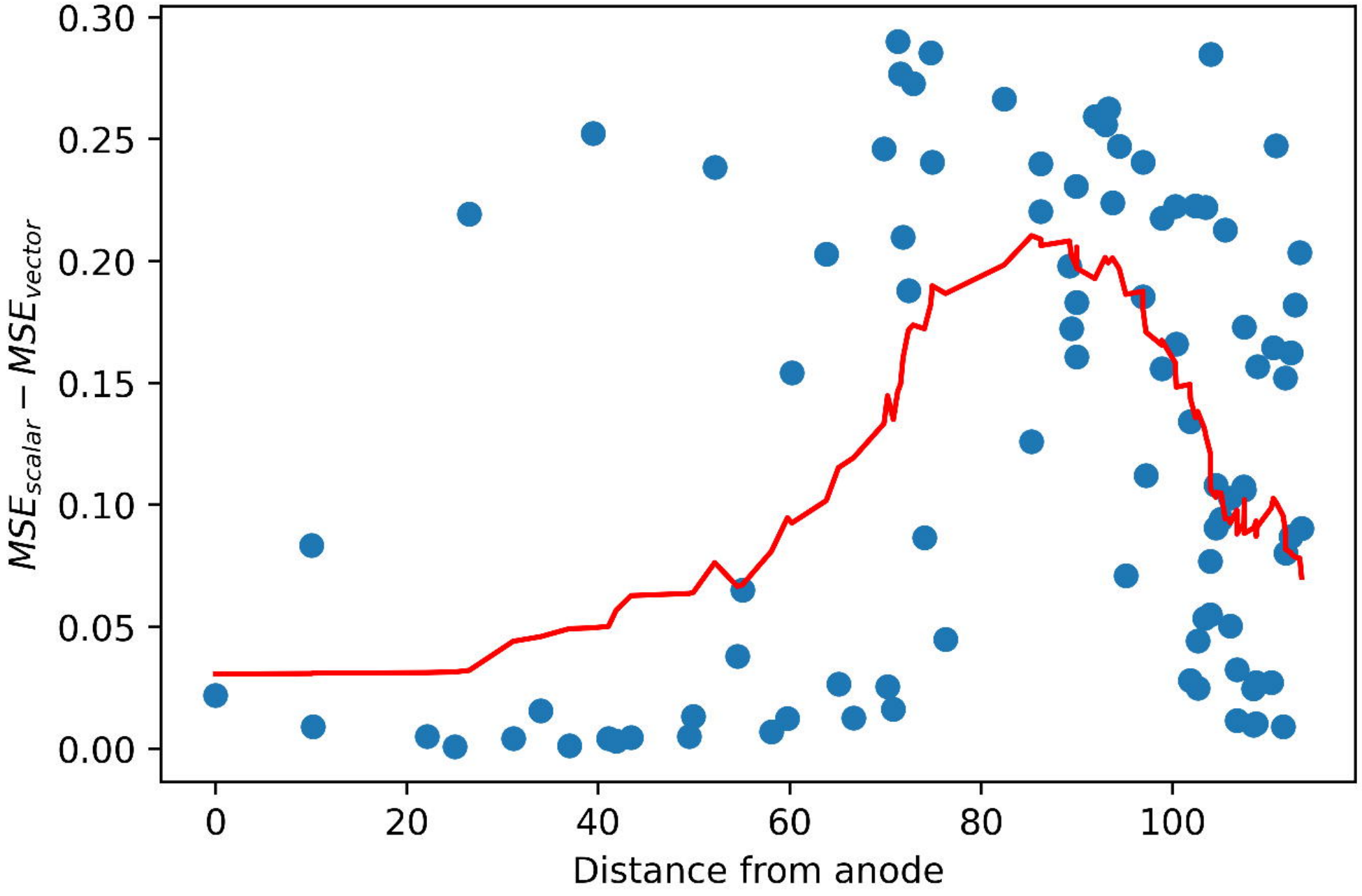
0.30
0.25
0.20
0.15
0.10
0.05
0.00
$MSE_{scalar} - MSE_{vector}$
0
20
40
60
80
100
Distance from anode

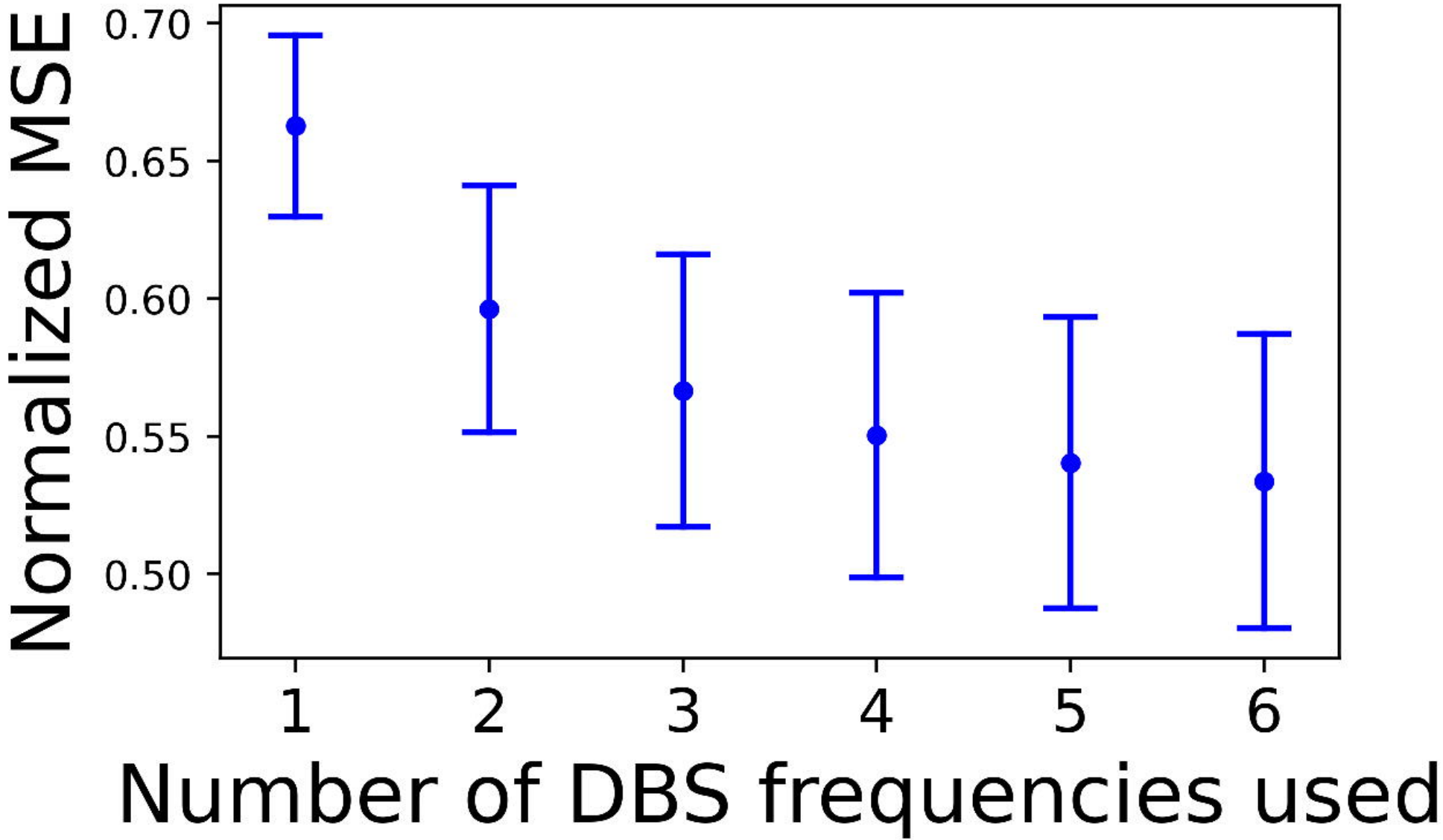
Normalized MSE
0.70
0.65
0.60
0.55
0.50
1
2
3
4
5
6
Number of DBS frequencies used

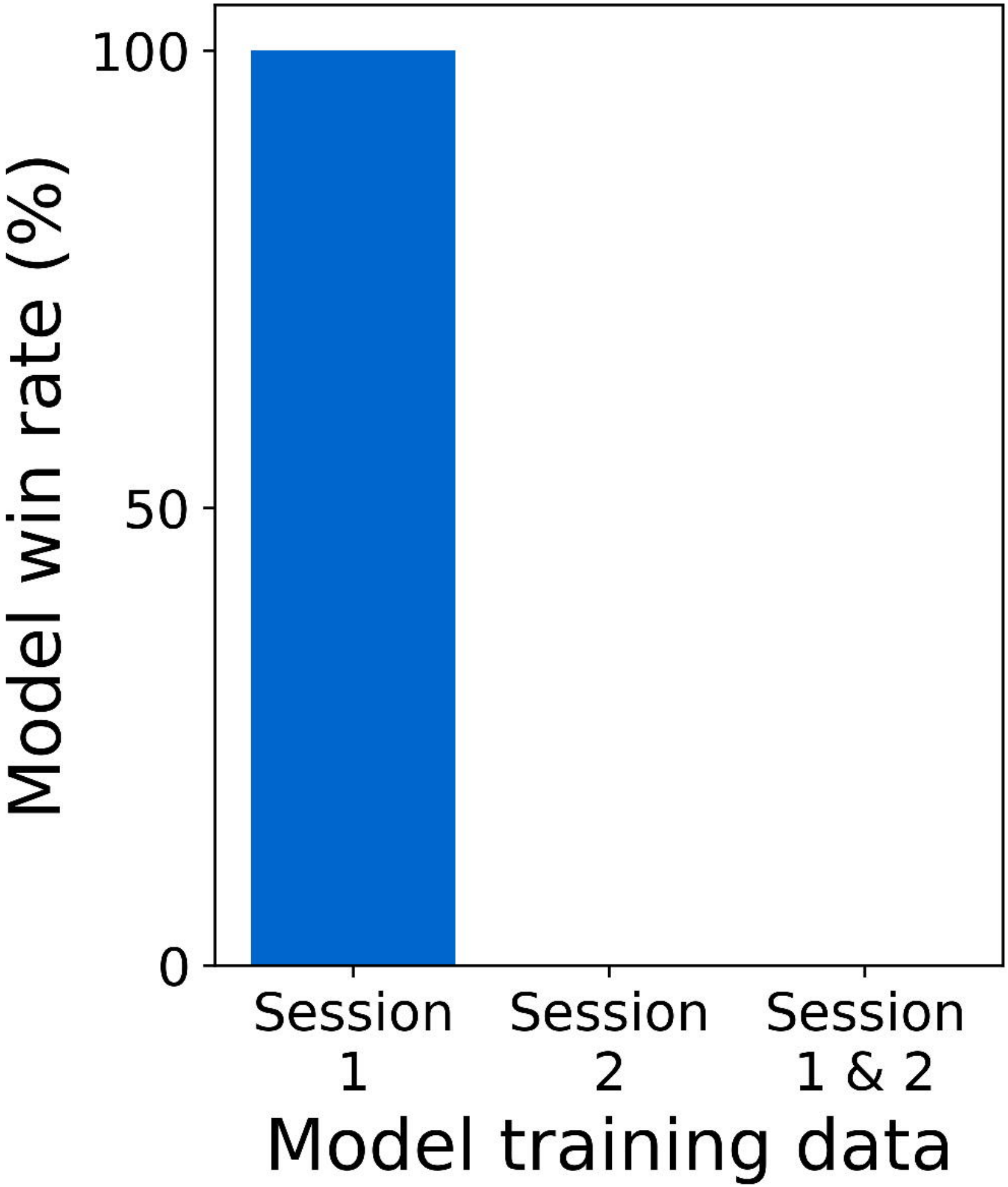
100
50
0
Model win rate (%)
Session 1
Session 2
Session 1 & 2
Model training data